Original Article

MOLECULAR METABOLISM

Insulin resistance is mechanistically linked to hepatic mitochondrial remodeling in non-alcoholic fatty liver disease

Chris E. Shannon [1], Mukundan Ragavan [2], Juan Pablo Palavicini [1,3], Marcel Fourcaudot [1], Terry M Bakewell [1], Ivan A. Valdez [1], Iriscilla Ayala [1], Eunsook S. Jin [4], Muniswamy Madesh [5], Xianlin Han [1,3,6], Matthew E. Merritt [2], Luke Norton [1,*]

ABSTRACT

Objective: Insulin resistance and altered hepatic mitochondrial function are central features of type 2 diabetes (T2D) and non-alcoholic fatty liver disease (NAFLD), but the etiological role of these processes in disease progression remains unclear. Here we investigated the molecular links between insulin resistance, mitochondrial remodeling, and hepatic lipid accumulation.

Methods: Hepatic insulin sensitivity, endogenous glucose production, and mitochondrial metabolic fluxes were determined in wild-type, obese (ob/ob) and pioglitazone-treatment obese mice using a combination of radiolabeled tracer and stable isotope NMR approaches. Mechanistic studies of pioglitazone action were performed in isolated primary hepatocytes, whilst molecular hepatic lipid species were profiled using shotgun lipidomics.

Results: Livers from obese, insulin-resistant mice displayed augmented mitochondrial content and increased tricarboxylic acid cycle (TCA) cycle and pyruvate dehydrogenase (PDH) activities. Insulin sensitization with pioglitazone mitigated pyruvate-driven TCA cycle activity and PDH activation via both allosteric (intracellular pyruvate availability) and covalent (PDK4 and PDP2) mechanisms that were dependent on PPARγ activity in isolated primary hepatocytes. Improved mitochondrial function following pioglitazone treatment was entirely dissociated from changes in hepatic triglycerides, diacylglycerides, or fatty acids. Instead, we highlight a role for the mitochondrial phospholipid cardiolipin, which underwent pathological remodeling in livers from obese mice that was reversed by insulin sensitization.

Conclusion: Our findings identify targetable mitochondrial features of T2D and NAFLD and highlight the benefit of insulin sensitization in managing the clinical burden of obesity-associated disease.

Keywords Insulin resistance; Metabolic liver disease; Mitochondria; Thiazolidinedione; Cardiolipin; Pyruvate dehydrogenase

1. INTRODUCTION

Patients with type 2 diabetes mellitus (T2D) are at increased risk of developing non-alcoholic fatty liver disease (NAFLD) and are more likely to progress toward the severe maladies of non-alcoholic steatohepatitis (NASH) and hepatocellular carcinoma [1,2]. Although the precise events linking T2D and NAFLD remain unclear, their shared association with obesity and insulin resistance suggests a common underlying pathology characterized by ectopic lipid accumulation and elevated rates of hepatic glucose production [3–5].

Studies in humans have identified alterations in hepatic mitochondria as a central feature of T2D and NAFLD [5,6]. Liver mitochondria integrate key metabolic pathways that, in addition to fueling oxidative metabolism, allow intermediates to move into (anaplerotic) and out of (cataplerotic) the tricarboxylic acid cycle (TCA) cycle to support biosynthetic processes, such as gluconeogenesis and lipogenesis. In rodent models of NAFLD, increased hepatic lipid delivery following an obesogenic diet enhances TCA cycle activity and anaplerotic/cataplerotic fluxes, which augments oxidative stress and inflammation [7,8]. Similarly, obese human subjects with insulin resistance display elevated rates of hepatic mitochondrial respiration, whereas this adaptive response to increased lipid availability is lost in patients who progress to develop NASH [9]. Thus, alterations in mitochondrial function are observed early in the pathogenesis of hepatic insulin resistance and steatosis, suggesting that targeting mitochondrial metabolism may be a viable treatment strategy to slow the progression of hepatic insulin resistance and NAFLD.

[1]Division of Diabetes, University of Texas Health Science Center and Texas Diabetes Institute, San Antonio, TX, USA [2]Department of Biochemistry and Molecular Biology, College of Medicine, University of Florida, Gainesville, FL, USA [3]Barshop Institute for Longevity and Aging Studies, University of Texas Health Science Center at San Antonio, San Antonio, TX, USA [4]Advanced Imaging Research Center, University of Texas Southwestern Medical Center, Dallas, TX, USA [5]Division of Nephrology, University of Texas Health Science Center and Texas Diabetes Institute, San Antonio, TX, USA [6]Glenn Biggs Institute for Alzheimer's & Neurodegenerative Diseases, University of Texas Health Science Center at San Antonio, San Antonio, TX, USA

*Corresponding author. Fax: +210 567 6554. E-mail: nortonl@uthscsa.edu (L. Norton).

Received December 7, 2020 • Revision received December 18, 2020 • Accepted December 20, 2020 • Available online 23 December 2020

https://doi.org/10.1016/j.molmet.2020.101154

The thiazolidinedione pioglitazone is the only FDA-approved insulin sensitizing agent established for the treatment of T2D [10—12]. Pioglitazone increases hepatic and peripheral insulin sensitivity and preserves β-cell function [13] and is highly effective at preventing the progression of pre-diabetes to T2D [14]. Pioglitazone also has shown remarkable promise in the treatment of steatosis, fibrosis, and inflammation in NAFLD and NASH. In the first placebo-controlled human trial, pioglitazone treatment for 6 months reduced hepatic steatosis, hepatocyte ballooning, and inflammation [15]. In long-term follow-up studies, pioglitazone treatment for 18 months led to further improvements in hepatic fibrosis [12]. Most recently, it was demonstrated that resolution of NASH occurred in a significant number of patients who took pioglitazone for 18 months compared to subjects undergoing lifestyle interventions [11]. Despite the effectiveness of pioglitazone toward multiple defects associated with T2D, NAFLD, and NASH, the precise mechanisms governing the impact of insulin sensitization on these abnormalities in liver remain unclear.

Although typically ascribed to adipose tissue PPARγ-mediated reductions in systemic lipid concentrations and ectopic lipid accumulation [16—18], the disease-modifying effects of pioglitazone may also involve direct effects on liver metabolism. For example, pioglitazone acutely suppresses glucose production in cultured hepatocytes [19,20] and perfused livers [21] and was recently found to decrease liver TCA cycle flux in a mouse model of NAFLD [22]. Consistent with an effect of insulin sensitizers on mitochondrial function, data from our lab [19] and others [23] indicate that thiazolidinediones may directly inhibit mitochondrial pyruvate flux in hepatocytes.

Therefore, in the present study, we tested the hypothesis that insulin sensitization with pioglitazone ameliorates NAFLD in obese mice by targeting mitochondrial pyruvate metabolism in liver. Using a combination of $^{2}H/^{13}C$ NMR metabolic flux analyses, high-resolution shotgun lipidomics, and molecular approaches, our findings confirm that obese mice display elevated rates of oxidative metabolism and reveal that improvements in insulin sensitivity driven by pioglitazone are closely linked to the suppression of mitochondrial pyruvate metabolism and TCA cycle activity. We further highlight that these effects of pioglitazone occur in the context of significant hepatic mitochondrial remodeling and are completely independent of reductions in liver fat content. Together, these data highlight the importance of hepatic mitochondrial function as a potential therapeutic target for the treatment of T2D and NAFLD.

2. MATERIALS AND METHODS

2.1. Experimental models and animal details

2.1.1. Animal studies

Eight-week-old wild-type (C57BL/6J; JAX #000664) and ob/ob (B6 ob; JAX #000632) male mice were purchased from The Jackson Laboratory, housed in environmentally-controlled conditions (23 °C, 12-hour light/dark cycles) and provided ad-libitum access to water and a control (70% kcal carbohydrate, 10% kcal fat, 20% kcal protein; D12450J; Research Diets, Inc., NJ, USA) or macronutrient-matched diet supplemented with pioglitazone (300 mg/kg; D17010703; Research Diets, Inc.). Experiments were conducted in 12- to14-week-old mice following four weeks of diet treatments. For high-fat diet experiments, 12-week-old C57BL/6J mice were fed chow diet or 60% kcal fat diet (D12492; Research Diets, Inc.) for 9 months. All procedures were approved by the Institutional Animal Care and Use Committee at the University of Texas Health Science Center at San Antonio.

2.1.2. Cell culture

Primary hepatocytes were isolated from 12- to 16-week-old wild-type male mice and maintained in serum-free Dulbecco's modified Eagle's medium (DMEM) supplemented with Pen-Strep (50 U/ml; Gibco, CA, USA). 5×10^5 cells were seeded in collagen-coated 6-well plates (354400; Corning) and treated with pioglitazone (2.5—10 μM) or vehicle control (0.01% dimethyl sulfoxide (DMSO)) for 0—24 h. For transcriptional inhibition experiments, actinomycin D was added to cells (0.5 μg/ml) 1 h prior to treatment with pioglitazone or vehicle for 6 h. For siRNA transfection experiments, 25 pmols (final concentration 12.5 nM) of Dharmacon SmartPool siSCR (#D-001810-10-05) or siPPARγ (#L-040712-00-0005) were delivered to cells with 9 μl of Lipofectamine® RNAiMAX reagent (#13778; ThermoFisher, MA, USA) in accordance with the manufacturer's recommendations 4 h after plating. Treatments were added 18—24 h after plating.

2.2. Method details

2.2.1. Oral glucose tolerance test

Overnight-fasted (16 h) ob/ob mice fed control (OB-CON) or pioglitazone (OB-PIO) diet were administered with a fixed dose of 50 mg of glucose (250 μl of 20% dextrose) by oral gavage. Glucose concentration was determined in whole blood sampled at baseline and at 15-, 30-, 60-, and 120-minute intervals from a tail incision using a glucometer (Contour next EZ).

2.2.2. Endogenous glucose production

Overnight-fasted OB-CON and OB-PIO mice were infused with 3-^{3}H glucose (0.1 μCi/min) for 2 h through a jugular vein catheter that had been inserted five days prior to experiments. Blood was sampled at −20, −10, 0, 90, 100, 110, and 120 min for the measurement of plasma glucose specific activity.

2.2.3. Peripheral insulin sensitivity

For euglycemic-hyperinsulinemic clamp studies in OB-CON and OB-PIO mice, insulin was infused at a constant rate (5 mU/kg/min) and blood was sampled every 5 min to monitor glucose concentrations. Glucose (20% glucose) was infused at a variable rate to maintain euglycemia at 100 mg/dL and red blood cells from donor mice were infused continuously to prevent anemic volume depletion. A 3-^{3}H glucose tracer was infused continuously (0.1 μCi/min) for the determination of insulin-stimulated glucose output.

2.2.4. Body composition

Lean mass, fat mass, and total body water were determined in OB-CON and OB-PIO mice by quantitative magnetic resonance imaging (qMRI) at the San Antonio Nathan Shock Center Aging Animal Models and Longevity Assessment Core.

2.2.5. Plasma analytes

Plasma insulin was determined by enzyme-linked immunosorbent assay (ELISA, #90080; Crystal Chem, IL, USA). Plasma free fatty acids (999—34691; FUJIFILM Wako Chemicals; VA, USA), glycerol (F6428; Sigma, MO, USA), and triglycerides (TR22421; ThermoFisher, MA, USA) were determined by enzymatic calorimetric assay.

2.2.6. Liver citrate synthase activity

Citrate synthase activity was determined in liver homogenates by spectrophotometric assay, which monitors the rate of CoASH formation from the condensation of oxaloacetate with acetyl-CoA in the presence

of the 5,5-dithio-bis-2-nitrobenzoic acid [24]. Data were normalized to homogenate protein content (BCA assay; ThermoFisher).

2.2.7. Western blotting and quantitative real-time polymerase chain reaction (qRT-PCR)

Immunoblot analysis was carried out on cell or liver lysates using primary antibodies from Cell Signaling Technologies (VDAC1 #4661; citrate synthase #14309; IDH2 #56439; SDHA #11998; PDH E1α #3205; PPARγ #2435; FABP4 #2120) and Abcam (COX IV #14744; β-Tubulin 179513; PDK4 #214938; PDP2 #233517) and developed by chemiluminescence method (ECL). QRT-PCR was performed using pre-designed TaqMan probes (Life Technologies, CA, USA) or SYBR green primer assays (Integrated DNA Technologies, Iowa, USA). Data were normalized to the geometric mean of the reference genes *B2m*, *Hmbs,* and *β-actin*.

2.2.8. Multi-dimensional mass spectrometry-based shotgun lipidomics

Liver tissue was lyophilized and homogenized in ice-cold diluted phosphate-buffered saline (0.1$\times$ PBS). Lipids were extracted by a modified procedure of Bligh and Dyer extraction in the presence of internal standards, which were added based on total protein content as previously described [25,26]. A triple-quadrupole mass spectrometer (Thermo Scientific TSQ Altis, CA, USA) and a Quadrupole-Orbitrap™ mass spectrometer (Thermo Q Exactive™) equipped with a Nanomate device (Advion Bioscience Ltd., NY, USA) and Xcalibur system software was used as previously described [27]. Briefly, diluted lipid extracts were directly infused into the electrospray ionization source through a Nanomate device. Signals were averaged over a 1-minute period in the profile mode for each full-scan mass spectrometry (MS) spectrum. For tandem MS, a collision gas pressure was set at 1.0 mTorr, but the collision energy varied with the classes of lipids. Similarly, a 2- to 5-minute period of signal averaging in the profile mode was employed for each tandem MS mass spectrum. All full and tandem MS mass spectra were automatically acquired using a customized sequence subroutine operated under Xcalibur software. Data processing, including ion peak selection, baseline correction, data transfer, peak intensity comparison, 13C deisotoping, and quantitation, were conducted using a custom programmed Microsoft Excel macro as previously described after considering the principles of lipidomics [28].

2.2.9. ^{13}C and ^{2}H tracer studies

For the assessment of fractional glucose production and mitochondrial pyruvate metabolism, overnight-fasted mice were administered with 27 μl/g body weight of $^{2}H_2O$ (99.9%; Cambridge Isotopes) by intraperitoneal injection. Thirty minutes after the $^{2}H_2O$ injection, mice were anesthetized with isoflurane and injected with 30 μmols [2,3—^{13}C] of pyruvate (Cambridge Isotopes) in 150 μl of saline. Eight minutes after [2,3—^{13}C] pyruvate injection, livers were freeze-clamped *in situ,* and blood was collected by cardiac puncture. A portion of liver was pulverized under liquid nitrogen, extracted in ice-cold perchloric acid, neutralized with potassium hydroxide and lyophilized in preparation for glutamate isotopomer analysis. Plasma was isolated from whole blood by centrifugation and used for the preparation of monoacetone glucose.

2.2.10. ^{13}C NMR analysis of liver glutamate isotopomers

^{13}C NMR spectra were acquired using an NMR spectrometer interfaced with a 14.1 T magnet equipped with a home-built superconducting (HTS) probe [29]. NMR samples were prepared by dissolving the lyophilized powder from PCA extraction in 90% (v/v) of 50 mM sodium phosphate in $^{2}H_2O$ (pH 7.0) containing 2 mM of ethylenediaminetetraacetic acid (EDTA). To this solution, 10% (v/v) internal standard containing 5 mM DSS-d6 and 0.2% (w/v) NaN_3 in $^{2}H_2O$ was added. ^{13}C spectra were measured with a spectra width of 240 ppm and an acquisition time of 1.5 s at 298 K. ^{1H}decoupling was performed using WALTZ-16 scheme. ^{13}C NMR spectra were processed (zero filled to 131,072 points, 0.5 Hz exponential line broadening, and polynomial baseline correction) using Mestrenova (v13.0 or above). Chemical shift referencing was carried out by setting taurine resonance to 48.4 ppm. Glutamate resonances were identified and fitted to mixed Gaussian/Lorentzian line-shapes, and peak areas were obtained.

2.2.11. Synthesis of monoacetone glucose (MAG)

To the plasma, barium hydroxide (0.05 M) and zinc sulphate (0.1 M) solutions were added, vortexed, and centrifuged. The supernatant was separated and lyophilized. To the lyophilized powder, a mixture of acetone and concentrated sulfuric acid was added and vortexed for 4 h. After 4 h, 1.5 M of sodium carbonate was added to adjust the pH to 1.75 and stirred for 24 h. This solution was then lyophilized, and MAG was extracted with ethyl acetate and dried under a stream of nitrogen.

2.2.12. ^{13}C and ^{2}H NMR analysis of MAG

Samples of synthesized MAG were dissolved in a mixture containing 94% (v/v) CD_3CN and 6% (v/v) $^{2}H_2O$. ^{13}C NMR spectra of MAG were recorded and processed with the same parameters as those used for recording the PCA extracted samples. Chemical shift referencing was carried out by setting the central acetonitrile resonance to 1.3 ppm. All other processing steps were identical to those used to analyze glutamate isotopomers. ^{2}H NMR spectra were measured using an NMR spectrometer (14.1 T magnet) equipped with a 3 mm broadband probe with a spectral width of 10.5 ppm and an acquisition time of 1 s at 323 K. ^{2}H NMR spectra were processed using a 2 Hz exponential line broadening and polynomial baseline correction. Chemical shifts were referenced by setting the acetonitrile resonances to 1.97 ppm. Fractional contributions to glucose production by the livers were estimated using a Bayesian approach described elsewhere [30].

2.2.13. Pyruvate dehydrogenase activation status

The activation status of pyruvate dehydrogenase was assayed in liver homogenate from a portion of the left lobe of the liver that had been freeze-clamped *in situ* in isoflurane-anesthetized mice. The rate of acetyl-CoA production from pyruvate was monitored over 10 min at 37° in a buffer containing NAD^+, coenzyme A, and thiamine pyrophosphate, as well as the PDK and PDP inhibitors dichloroacetate and sodium fluoride, respectively [31,32].

2.2.14. Liver metabolite analyses

A 50-mg portion of freeze-clamped liver from isoflurane-anesthetized mice was lyophilized overnight and acid-soluble metabolites were subsequently extracted in 0.5 M perchloric acid. Acetyl-CoA and CoASH were assayed by radioenzymatic assay [33]. Lactate was assayed by the fluorometric detection of NADH in the presence of excess concentrations of NAD^+, hydrazine and lactate dehydrogenase [34]. Glucose-6-phosphate (G6P) was assayed by the fluorometric detection of NADH in the presence of 50 mmol/L of triethanolamine, 0.5 mmol/L of dithiothreitol, 0.25 mmol/L of ATP, 1 mmol/L of NAD, and 0.6 units of bacterial G6PDH (G5760; Sigma—Aldrich).

2.2.15. Hepatic glycogen synthesis

Livers harvested from anesthetized mice following 3-^{3}H infusion during euglycemic clamp were used to estimate rates of plasma glucose incorporation into liver glycogen. A 20-mg portion of liver was alkaline digested at 85° for 30 min, allowed to cool, and neutralized with hydrochloric acid. One half of the neutralized extract was treated with amyloglucosidase for 1 h at room temperature. The liberated glucose was subsequently measured in an aliquot of each extract. Five volumes of ethanol were added to the remaining extract to precipitate glycogen. The glycogen pellet was further washed in ethanol, solubilized in water and added to scintillation vials for radioactivity counting. The specific activity was measured as DPM/glycogen and was normalized to plasma tritium specific activity to estimate glycogen synthesis rates during the entire clamp period.

2.3. Quantification and statistical analyses

Differences between WT, OB-CON, and OB-PIO groups were assessed using one-way analysis of variance, with individual differences isolated post-hoc using the Tukey test. For analyses in which no wild-type groups were included, differences between OB-CON and OB-PIO were assessed using unpaired t-testing. Significance testing was performed using GraphPad Prism 7. Data are presented as mean ± standard error, and data were considered significantly different at $P < 0.05$.

3. RESULTS

3.1. Effects of insulin sensitivity on pathways of hepatic glucose production

As the first step to dissect the impact of insulin sensitivity on hepatic mitochondrial metabolism, we initially explored the effects of a pioglitazone enriched diet (300 ppm) on sources of liver glucose production in ob/ob mice (OB-PIO) compared to ob/ob mice fed a matched control diet (OB-CON). In overnight fasted mice, basal endogenous glucose production (EGP) measured from [$^{3}H_3$]glucose dilution was 35% lower in OB-PIO compared to OB-CON (Figure 1A). This was associated with improvements in glucose homeostasis (Figure 1B and Supplemental Figure 1) and whole-body (Figure 1C) and liver-specific (Figure 1D) insulin sensitivity. Consistent with human studies [10,35], insulin sensitization with OB-PIO mice occurred despite significantly greater weight gain and fat mass (Supplemental Table 1). Importantly, the effects of pioglitazone on total EGP was not due to changes in the cytosolic redox state, a key driver of EGP [36], as the hepatic lactate/pyruvate ratio was unaltered by pioglitazone (Figure 1E). Moreover, EGP reduction by pioglitazone could not be explained by effects on adipose tissue lipolysis, (i.e., indirect regulation of EGP), since circulating levels of free fatty acids and glycerol were similar in OB-CON and OB-PIO mice (Supplemental Table 1). Accordingly, hepatic glycerol concentrations (the primary adipose-derived source of glucose production) were also unchanged by pioglitazone treatment (Supplemental Figure 1B), demonstrating that, similarly to the effects of insulin [37], pioglitazone suppresses EGP through direct actions on the liver rather than indirectly through the regulation of circulating substrate availability.

We next explored which hepatic pathways were involved in the modulation of glucose metabolism by pioglitazone. Total EGP is the summed contributions from i) the breakdown of stored glycogen (glycogenolysis), ii) gluconeogenesis from glycerol ($GNG_{glycerol}$), and iii) gluconeogenesis from the anaplerotic/cataplerotic generation of phosphoenolpyruvate (GNG_{PEP}) [30]. To determine the fractional contributions from glycogenolysis, $GNG_{glycerol}$, and GNG_{PEP} to total

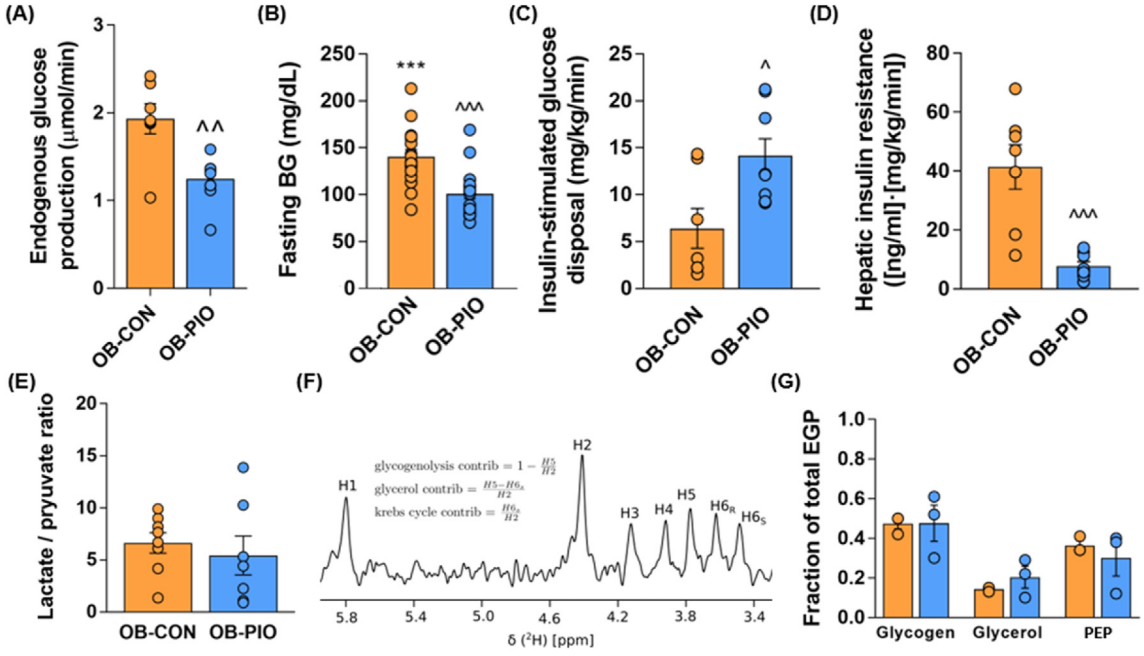

Figure 1: Effect of insulin sensitivity on pathways of hepatic glucose production. **(A)** Endogenous glucose production measured using 3-^{3}H glucose, **(B)** fasting blood glucose, **(C)** whole-body insulin sensitivity assessed during euglycemic-hyperinsulinemic clamp, **(D)** hepatic insulin-resistance index (fasting plasma insulin multiplied by basal endogenous glucose production), and **(E)** hepatic lactate/pyruvate ratio in overnight-fasted untreated obese mice (OB—CON) and obese mice treated with pioglitazone (20 mg/kg/day) for 4 weeks (OB-PIO). **(F)** Representative mono-acetone glucose ^{2}H NMR spectra derived from plasma glucose of fasted mice. **(G)** Fractional contribution from glycogenolysis (1-[H5/H2]), glycerol-driven gluconeogenesis ([H5−$H6_S$]/H2) and PEP-driven gluconeogenesis ($H6_S$/H2) to total endogenous glucose production in OB-CON and OB-PIO mice, calculated from mono-acetone glucose ^{2}H NMR spectra. Data are mean ± SE for at least 5 mice per group, as indicated on individual figure panels, except (G), which is n = 3. ^P < 0.05, ^^P < 0.01, ^^^P < 0.001 vs OB-CON.

EGP, plasma was collected from mice administered with $^{2}H_2O$. NMR analysis of the ^{2}H spectra in monoacetone glucose revealed that the relative contribution from these different pathways to EGP was similar between OB-CON and OB-PIO mice (Figure 1F,G). Together, these data demonstrate that 4 weeks of pioglitazone treatment suppressed several contributing pathways of EGP without altering the hepatic redox state or adipose-derived substrate availability.

3.2. Hepatic mitochondrial remodeling in insulin resistance

Several studies have reported that mice with insulin resistance and NAFLD display increased hepatic mitochondrial content and excessive oxidative metabolism [38,39]. As this may be an important contributor to the exaggerated rates of EGP in NAFLD, we investigated the relationship between insulin resistance and hepatic mitochondrial remodeling. To investigate hepatic mitochondrial mass, we first compared the mitochondrial marker enzyme citrate synthase in livers from OB-CON with those from age-matched wild-type control mice (WT). Both the maximal activity (Figure 2A) and protein content (Figure 2B,C) of citrate synthase were elevated in OB-CON compared to WT mice. Other protein markers of hepatic mitochondrial mass were also increased in OB-CON mice, including enzymes of the TCA cycle (isocitrate dehydrogenase 2 [IDH2]) and electron transport chain (cytochrome C oxidase IV [COX IV]), whereas the outer mitochondrial membrane protein VDAC1 and complex II protein (succinate dehydrogenase [SDHA]) were unchanged (Figure 2B,C). Insulin sensitization with pioglitazone largely restored citrate synthase activity (Figure 2A) and COX IV protein levels (Figure 2B,C) but had no impact on other protein markers of mitochondrial mass (Figure 2B,C). These data demonstrate that mitochondrial mass and oxidative capacity are increased in the livers of obese mice, while the normalization of citrate synthase activity in OB-PIO mice suggests that pioglitazone may induce intrinsic remodeling of mitochondria independent of significant changes in mitochondrial mass.

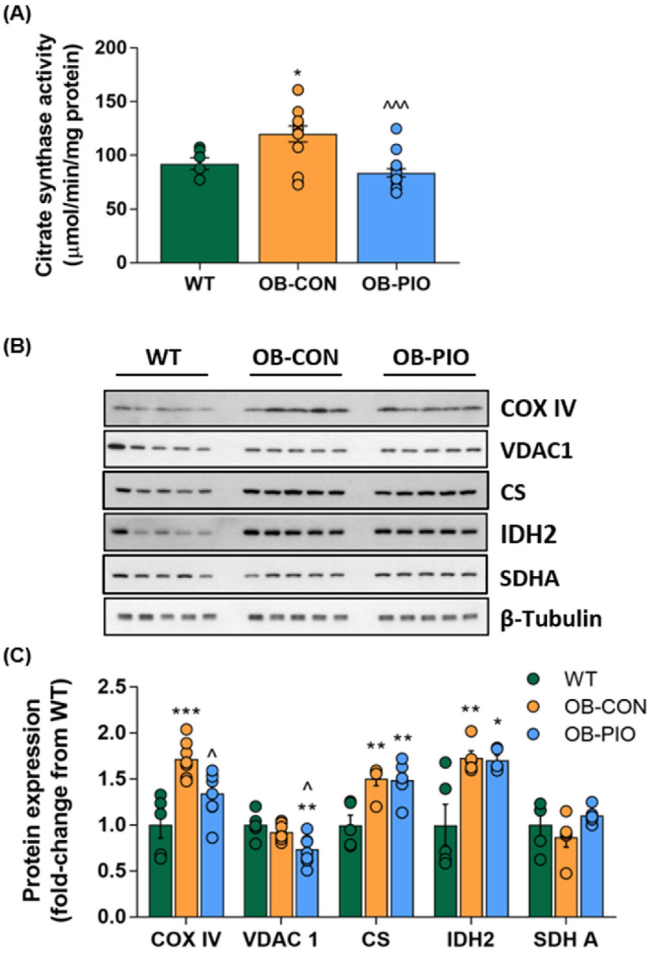

Figure 2: Hepatic mitochondrial remodeling in insulin resistance. **(A)** Hepatic citrate synthase activity measured spectrophotometrically, **(B)** representative western blots, and **(C)** quantified densitometry of mitochondrial proteins cytochrome C oxidase IV (COX IV), voltage-dependent anion channel 1 (VDAC1), citrate synthase (CS), isocitrate dehydrogenase 2 (IDH2), and succinate dehydrogenase alpha subunit (SHD A), normalized to β−tubulin control (relative to wild-type mice) in livers from wild-type, untreated obese mice (OB−CON), and obese mice treated with pioglitazone (20 mg/kg/day) for 4 weeks (OB-PIO). Data are mean ± SE for at least 5 mice per group, as indicated on individual figure panels. *P < 0.05, **P < 0.01, ***P < 0.001 vs WT; ^P<0.05, ^^^P<0.001 vs OB-CON.

3.3. Insulin sensitization suppresses mitochondrial pyruvate metabolism and TCA cycle activity

Because pioglitazone normalized hepatic citrate synthase activity, the rate-limiting enzyme of the TCA cycle [40], we next explored the relationship between TCA cycle fluxes and the glucose-lowering effects of pioglitazone. Pathways of TCA cycle anaplerosis and cataplerosis contribute to EGP through GNG_{PEP}, and scaling the fractional contribution of GNG_{PEP} to total EGP (Figure 1G,A) demonstrated that absolute rates of GNG_{PEP} fell from 0.7 μmol/min in OB-CON to 0.37 μmol/min in OB-PIO mice. The main anaplerotic fuels for liver mitochondria are pyruvate (via pyruvate carboxylase [PC]) and glutamine (through glutaminolysis), but only PC contributes appreciably to hepatic GNG_{PEP} in mice [41]. To dissect the effect of hepatic insulin sensitization on mitochondrial pyruvate metabolism and PC flux *in vivo*, we administered mice with a bolus injection of [2,3—^{13}C] pyruvate and harvested plasma and livers 8 min later. Plasma signals from [1,2—^{13}C2] and [5,6—^{13}C2]glucose isotopomers were more prominent in OB-CON compared to OB-PIO mice (Supplemental Figure 2). Since these isotopomers reflect the direct pathway of pyruvate-driven gluconeogenesis through PC (ref. [42] and Figure 3A), this result is consistent with reduced flux through PC contributing to the suppression of GNG_{PEP} in OB-PIO mice. However, we also observed doublets from [2,3—^{13}C2] and [3,4—^{13}C2]glucose isotopomers in plasma from OB-CON, which were markedly reduced in OB-PIO mice (Figure 3B). These doublets can only be produced by pyruvate carboxylation and subsequent turns of the TCA cycle (Figure 3A). Under the non-steady state conditions employed here, differential enrichment of these plasma glucose isotopomers following [2,3—^{13}C]pyruvate metabolism could reflect i) shifts in the balance between PC flux and pyruvate oxidation through pyruvate dehydrogenase (PDH), ii) altered rates of pyruvate cycling, and/or iii) lower TCA cycle turnover.

To evaluate the balance between PC (anaplerosis) and PDH (pyruvate oxidation) fluxes, we determined the ratio of hepatic [2,3—^{13}C]/[4,5—^{13}C] glutamate isotopomers in freeze-clamped livers from mice following the [2,3—^{13}C]pyruvate tracer experiment described above (see schematic in Figure 3C). This metric of PC/PDH was remarkably stable between OB-CON and OB-PIO mice under both basal and insulin-stimulated conditions (Figure 3D), demonstrating that although pioglitazone reduced GNG_{PEP} and PC fluxes, it did not alter the relative balance between pyruvate anaplerosis and pyruvate oxidation. Next, we explored the role of pyruvate cycling by monitoring the formation of

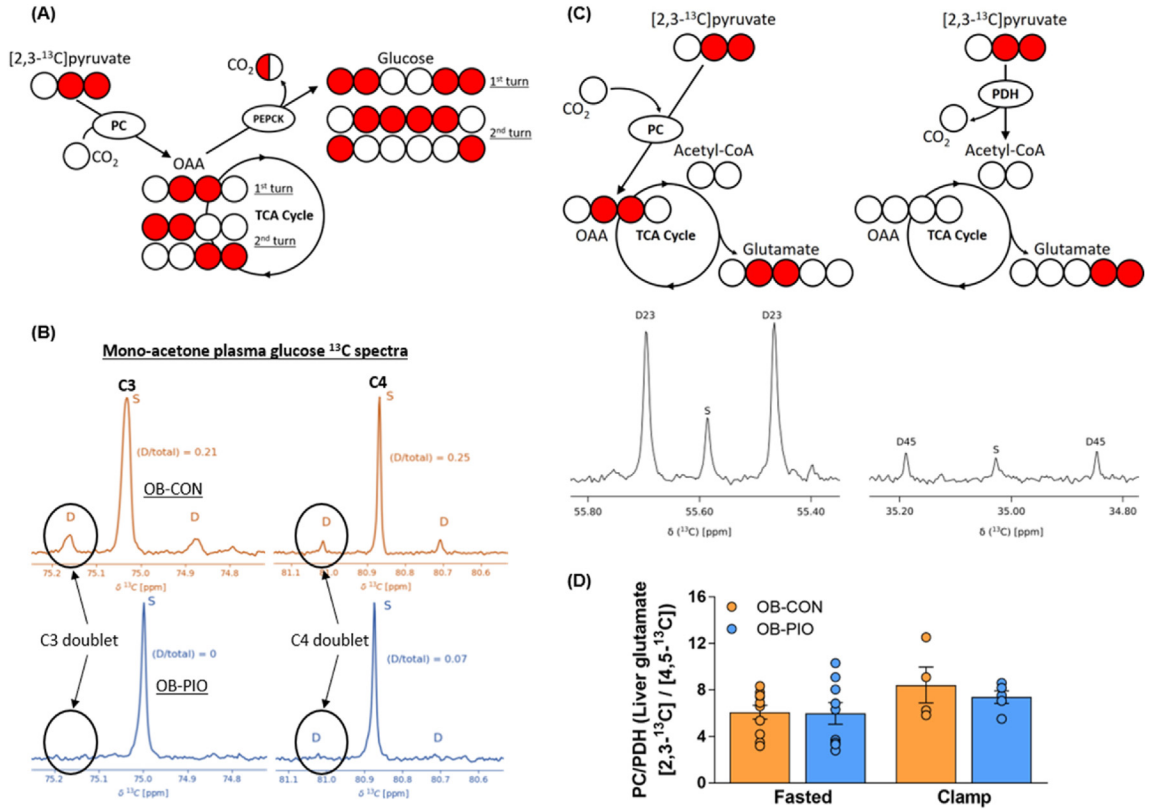

Figure 3: Insulin sensitization suppresses mitochondrial pyruvate metabolism and TCA cycle activity: (A) Schematic illustrating the labelling pattern of plasma glucose following administration of [2,3—^{13}C] pyruvate. PC-dependent gluconeogenesis generates predominantly [1,2—^{13}C] and [5,6—^{13}C] glucose isotopomers, but carbon scrambling through additional TCA cycle turnover can yield enrichment at interior glucose carbons (i.e., [2,3—^{13}C] and [4,5—^{13}C] isotopomers). PC pyruvate carboxylase, PEPCK pyruvate carboxykinase. **(B)** ^{13}C spectra showing augmented C-3 (left) and C-4 (right) resonance of monoacetone glucose synthesized from plasma in OB-CON (top) compared to OB-PIO (bottom) mice. **(C)** Schematic (top) showing determination of the ratio between pyruvate carboxylase (PC) and pyruvate dehydrogenase (PDH) flux from the labeling pattern of liver glutamate following [2,3—^{13}C] pyruvate metabolism through either PC (left panel, yielding [2,3—^{13}C] glutamate) or PDH (right panel, yielding [4,5—^{13}C] glutamate) and representative glutamate ^{13}C NMR spectra (bottom). **(D)** Quantified ratio of liver PC/PDH, reflecting relative mitochondrial anaplerotic/oxidative fluxes determined in OB-CON and OB-PIO mice in basal state and during hyperinsulinemic-euglycemic clamp. Data are mean ± SE.

hepatic ^{13}C2 lactate isotopomers. Cycling of [2,3—^{13}C]pyruvate through PC, equilibration in the 4-carbon TCA cycle intermediates and subsequent flux through PEP carboxykinase, pyruvate kinase, and lactate dehydrogenase, will produce [1,2—^{13}C2]lactate [43]. These lactate isotopomers were not observed in the ^{13}C spectra from either OB-CON or OB-PIO and, therefore, eliminated this pathway as a significant contributor to the reduction in GNG_{PEP}. Given that the PC/PDH ratio and rate of pyruvate cycling were both similar between groups, the suppression of [2,3—^{13}C2] and [3,4—^{13}C2]glucose isotopomers following [2,3—^{13}C]pyruvate metabolism can only reflect a down-regulation of TCA cycle turnover in OB-PIO mice. This result, which is consistent with the observed blunting of citrate synthase activity (Figure 2A) and a prior report [22], suggests that decreasing TCA cycle turnover is an important mechanism through which insulin sensitization reduces anaplerotic pathways of endogenous glucose production (GNG_{PEP}).

3.4. Hepatic PDH is hyperactivated in obese mice and suppressed by insulin sensitization

Our observation that pioglitazone treatment reduced PC flux (Supplemental Figure 2) without impacting the relative PC/PDH flux ratio (Figure 3D) suggested that insulin sensitization with pioglitazone also targets PDH flux in liver. We found that protein levels of the PDH catalytic subunit E1α were increased by 70% in OB-CON mice compared to WT and remained elevated in OB-PIO mice (Figure 4A). However, the enzymatic activity of PDH is primarily controlled by its catalytic activation status, which we measured directly in *in situ* freeze-clamped livers. Strikingly, PDH activation status was 6-fold higher in OB-CON mice compared to WT (Figure 4B). Consistent with our NMR flux analyses, pioglitazone treatment reduced hepatic PDH activation in OB-PIO mice under basal conditions and in OB-PIO mice undergoing euglycemic-hyperinsulinemic clamp studies (Figure 4C). The activity of PDH is regulated allosterically by the ratio of acetyl-CoA to free coenzyme A (Acetyl-CoA/CoASH) [44]. Since hepatic acetyl-CoA metabolism may be disturbed under insulin-resistant conditions [38], we next measured acetyl-CoA and CoASH concentrations in *in situ* freeze-clamped livers using a sensitive radioenzymatic assay [33]. Acetyl-CoA (Figure 4D) and CoASH (Figure 4E) were decreased by 9-fold and 2-fold, respectively, in OB-CON compared to WT mice, resulting in a 3-fold reduction in acetyl-CoA/CoASH (Figure 4F). We also determined acetylcarnitine concentrations, which parallel changes in the mitochondrial acetyl-CoA pool via the carnitine acetyltransferase reaction [45]. Acetylcarnitine was 5-fold lower in livers from OB-CON versus WT mice (Figure 4G), providing independent validation of our

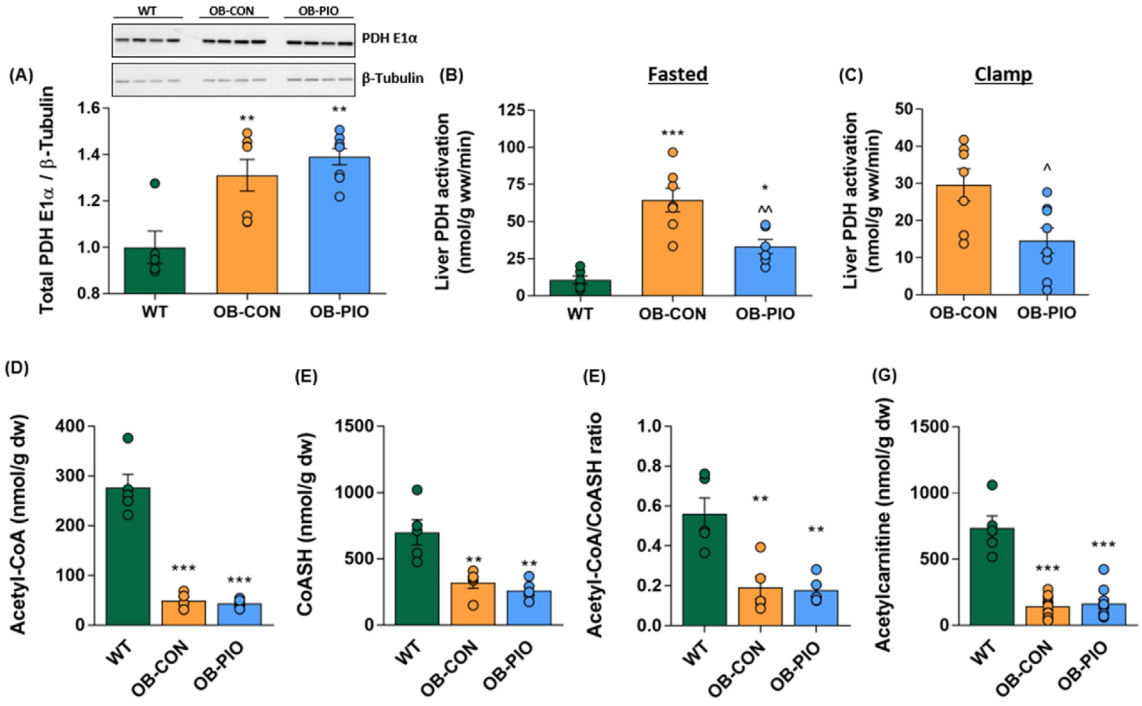

Figure 4: Hepatic PDH is hyperactivated in obese mice and suppressed by insulin sensitization. **(A)** Protein expression of the E1α catalytic subunit of the pyruvate dehydrogenase complex (normalized to β-tubulin control), normalized to wild-type levels in fasted WT, OB-CON, and OB-PIO mice, with representative blots. **(B)** Liver PDH activation measured in *in situ* freeze-clamped livers from overnight fasted OB-CON and OB-PIO mice. **(C)** Liver PDH activation in OB-CON and OB-PIO mice following insulin clamp. **(D)** Acetyl-CoA, **(E)** free coenzyme A, **(F)** acetyl-CoA/CoASH ratio and **(G)** acetylcarnitine concentrations in livers from overnight-fasted wild-type (WT), untreated obese (OB−CON) and pioglitazone-treated obese (OB-PIO) mice. *P < 0.05, **P < 0.01, P < 0.001 vs WT; ^P<0.05, ^^^P<0.001 vs OB-CON.

measurement of acetyl-CoA. This depletion of hepatic acetyl groups may thus contribute to the excessive PDH activity in livers from obese mice and is consistent with increased oxidative flux through the TCA cycle as observed in humans with NAFLD [38]. We next asked whether the restoration of hepatic acetyl-CoA levels could explain the lower PDH activity in pioglitazone-treated mice. However, insulin sensitization with pioglitazone had no impact upon hepatic acetyl-CoA concentrations, acetyl-CoA/CoASH or acetylcarnitine concentrations (Figure 4D−G).

3.5. Insulin sensitization reduces hepatic pyruvate availability

Alterations in hepatic acetyl-CoA disposal have previously been attributed to increased pyruvate availability in obese individuals [38]. Consistent with this, hepatic pyruvate concentrations were increased by 2.5-fold in OB-CON compared to WT mice and were completely normalized by pioglitazone treatment (Figure 5A). Since pyruvate is also an allosteric activator of PDH [46], changes in intracellular pyruvate availability likely represent another important mechanism linking insulin resistance with hepatic PDH and mitochondrial function. Hepatic pyruvate availability is determined by the balance between glycolytic pyruvate production, redox-dependent lactate dehydrogenase flux, and mitochondrial pyruvate disposal (i.e., PC vs PDH). Lactate concentrations were similar between fasted WT and OB-CON mice and were reduced following pioglitazone treatment (Figure 5B), while the lactate/pyruvate ratio (indicative of the cytosolic redox state) remained essentially unchanged across groups (Figure 1E). It is therefore unlikely that the decreased hepatic pyruvate in OB-PIO was due to increased pyruvate flux to lactate.

Both pyruvate and lactate availability are influenced by liver glycogen metabolism, which is often altered in models of obesity and liver disease [47,48]. Indeed, while liver glycogen was depleted in fasted WT mice, substantial hepatic glycogen remained in fasted OB-CON and OB-PIO mice (Figure 5C). As such, glycogenolysis accounted for approximately 50% of total glucose production in fasting OB-CON and OB-PIO mice (Figure 1G). Although fasting liver glycogen was no different between OB-CON and OB-PIO mice, scaling the ^{2}H NMR date from Figure 1G to total EGP (Figure 1A) indicated that absolute glycogenolysis was 50% lower in OB-PIO mice compared to OB-CON (0.92 vs 0.60 μmol/min). Importantly, however, the relative contribution of glycogenolysis to total EGP was not changed in obese mice treated with pioglitazone.

We also monitored the incorporation of plasma glucose into hepatic glycogen by infusing 3-^{3}H glucose under insulin clamp conditions in OB-CON and OB-PIO mice. Consistent with the marked hepatic insulin resistance observed in OB-CON (Figure 1D), liver glycogen synthesis from plasma glucose was negligible in these animals (Figure 5D). Insulin sensitization with pioglitazone resulted in a 10-fold increase in the incorporation of plasma glucose into liver glycogen (Figure 6D). Hepatic glucose-6-phosphate concentration, the primary allosteric effector of glycogen metabolism, was also 92% higher in OB-PIO mice (Figure 5E). Thus, excessive glycogen turnover may contribute to the elevation of hepatic pyruvate concentrations and activation of PDH in livers from insulin-resistant mice.

3.6. Pioglitazone induces hepatic PDK4 through PPARγ agonism

In addition to its allosteric control by acetyl-CoA and pyruvate, PDH is also under covalent regulation by the competing functions of inhibitory PDH kinases (PDKs) and activating PDH phosphatases (PDPs), with PDK4 and PDP2 being the isoforms of primary importance in murine liver [49,50]. Therefore, we sought to

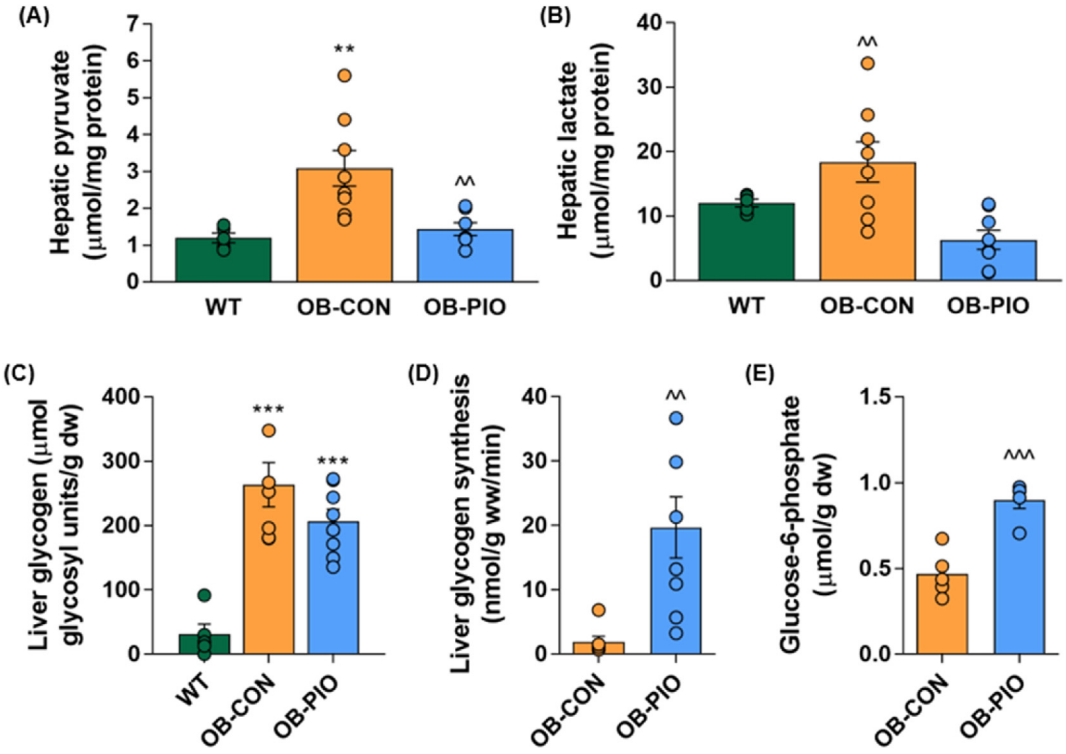

Figure 5: Insulin sensitization reduces hepatic pyruvate availability. **(A)** Hepatic pyruvate, **(B)** lactate, and **(C)** glycogen concentrations overnight-fasted wild-type (WT), untreated obese (OB—CON) and pioglitazone-treated obese (OB-PIO) mice. **(D)** Liver glycogen synthesis determined from 3 to 3H plasma glucose incorporation into hepatic glycogen during insulin clamp in OB-CON and OB-PIO mice. **(E)** Liver glucose-6-phosphate concentrations in in overnight-fasted OB-CON and OB-PIO mice. **P < 0.01, ***P < 0.001 vs WT; ^^P<0.01, ^^^P<0.001 vs OB-CON.

determine whether the increased PDH activation observed with hepatic insulin resistance might be additionally associated with changes in PDK4 and/or PDP2 expression. Under fasted conditions, hepatic PDK4 protein levels were reduced in OB-CON, while PDP2 levels were increased, compared to wild-type mice (Figure 6A—B). This pattern of increased PDP2 but suppressed PDK4 was largely mirrored in livers from wild-type mice fed a high-fat diet (Supplementary Figures 3A and 3B) and is expected to promote the conversion of PDH to its active form. Thus, perturbations in the covalent regulators of PDH likely contribute to the altered mitochondrial function with hepatic insulin resistance. Importantly, this reciprocal induction/suppression of PDP2 and PDK4 protein in OB-CON mice was reversed by pioglitazone treatment, both under basal and insulin-stimulated conditions (Figure 6A—B).

Although insulin sensitization by thiazolidinediones is believed to be mediated by predominant effects in adipose tissue [51], we have previously identified liver-centric actions of pioglitazone relevant to metabolic disease [19]. To investigate whether the regulation of PDK4 and PDP2 by pioglitazone could be due to direct effects on the liver parenchyma, we isolated primary hepatocytes from wild-type C57Bl/6 mice. Treatment of hepatocytes with 2.5 μM of pioglitazone resulted in a rapid (within 1 h) and sustained increase in *Pdk4* mRNA over 24 h (Figure 6C), which preceded a robust induction of PDK4 protein (Figure 6D,E). In contrast, no changes were observed in PDP2 expression following acute pioglitazone treatment (Supplemental Figure 3C). Because PDK4 is such a critical regulator of mitochondrial substrate selection and cellular metabolism [52], we next sought to identify the molecular mechanism responsible for its upregulation in pioglitazone-treated hepatocytes. Our time-course experiments (Figure 6C—E) suggested a transcriptional mode of regulation. In support of this, the increase in PDK4 protein with pioglitazone was blocked by the transcriptional inhibitor actinomycin D (Figure 6F). The major transcriptional target of thiazolidinediones in adipocytes is PPARγ [53] which, although expressed at very low levels in healthy hepatocytes [54,55], may become upregulated in NAFLD [55—57]. Interestingly, established PPARγ target genes *Cd36* and *Fabp4* mirrored the induction of *Pdk4* in pioglitazone-treated hepatocytes (Figure 6G,H), while FABP4 protein (Supplemental Figures 3D) and mRNA (Supplemental Figure 3E) levels were dramatically increased in livers from pioglitazone-treated obese mice. To explore whether PPARγ activation was indeed necessary for the induction of *Pdk4* by pioglitazone, we knocked down PPARγ in primary hepatocytes using siRNA-mediated gene silencing. This approach suppressed *Pparg* gene expression by 80% (Supplemental Figure 3F), effectively depleted PPARγ protein levels (Figure 6K), and blocked downstream *Pparg* target gene activation (Supplemental Figures 3G). Importantly, the increase in *Pdk4* mRNA (Figure 6I) and PDK4 protein (Figure 6J) following pioglitazone treatment was completely abolished in siPPARγ-transfected hepatocytes. These data thus demonstrate a requirement for PPARγ in the pioglitazone-driven induction of PDK4 *in vitro* and reveal an important mechanism through which pioglitazone modulates hepatic mitochondrial metabolism *in vivo*.

3.7. Hepatic insulin sensitization and mitochondrial lipid remodeling

Hepatic PPARγ activation, as observed in OB-PIO mice (Supplemental Figures 3D and E), is expected to promote hepatic lipid accumulation [58]. However, improvements in insulin sensitivity [12,59] and

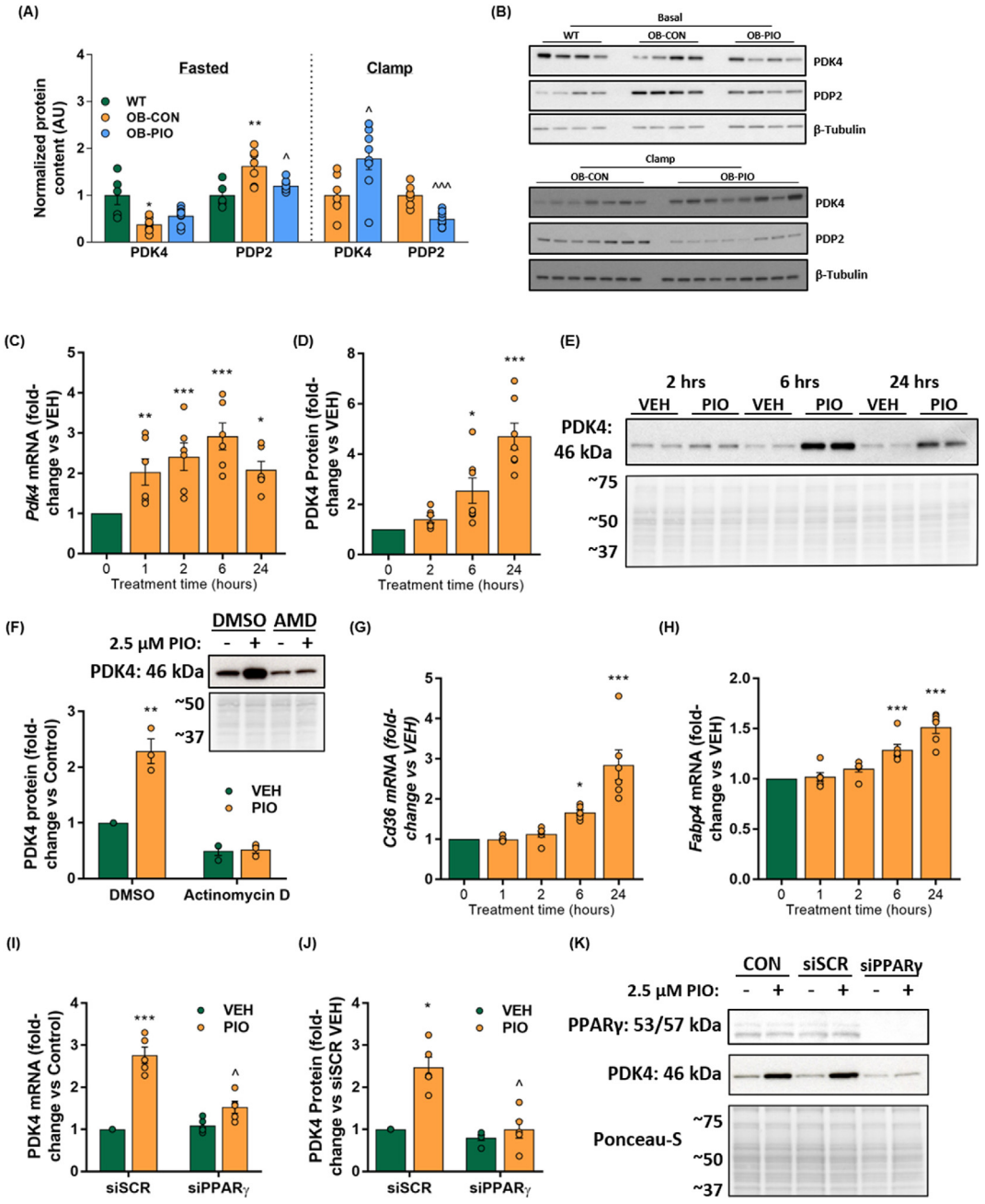

Figure 6: Pioglitazone induces hepatic PDK4 through PPARγ agonism. **(A)** Liver pyruvate dehydrogenase kinase 4 (PDK4) and pyruvate dehydrogenase phosphatase 2 (PDP2) protein expression in overnight-fasted WT, OB-CON, and OB-PIO mice and in OB-CON and OB-PIO mice following insulin clamp studies and (**B**) representative immunoblots. (**C**) mRNA, (**D**) protein, and (**E**) representative immunoblots of PDK4 expression in primary hepatocytes treated with 2.5 μM of pioglitazone for the indicative time periods. (**F**) PDK4 protein in primary hepatocytes treated with 2.5 μM of pioglitazone for 6 h in the absence or presence of the transcriptional inhibitor actinomycin D. (**G**) CD36 and (**H**) FABP4 mRNA expression in primary hepatocytes treated with 2.5 μM pioglitazone for the indicative time periods. (**I**) mRNA, (**J**) protein, and (**K**) representative immunoblots of PDK4 expression in primary hepatocytes transfected with siSCR or siPPARγ and treated with vehicle or 2.5 μM of pioglitazone for 6 h *P $<$ 0.05, **P $<$ 0.01, P $<$ 0.001 vs WT (**A** and **B**) or VEH; ^P$<$0.05, ^^^P$<$0.001 vs OB-CON (**A** and **B**) or siSCR (**I** and **J**).

mitochondrial function [22] following prolonged pioglitazone treatment are believed to occur secondarily to reduced ectopic lipid accumulation in liver and skeletal muscle [60]. To delineate this apparent paradox between hepatic lipid storage and mitochondrial metabolism, we examined liver fat content in obese mice treated with pioglitazone. This analysis revealed that total hepatic levels of triglycerides and free fatty acids (the quantitatively most important hepatic lipid classes) were unaffected or even tended to increase following pioglitazone treatment (Figure 7A and Supplemental Figure 4A). These data are consistent with chronic PPARγ activation in liver [58] but also demonstrate that improvements in hepatic insulin sensitivity, glucose homeostasis, and mitochondrial metabolism can be dissociated from bulk changes in liver fat content. Discrete lipid classes that have traditionally been linked with hepatic insulin resistance, including diacylglycerides and

long-chain acyl CoAs, also remained elevated following pioglitazone treatment (Figure 7B,C). In contrast, levels of hepatic ceramide were completely normalized by pioglitazone treatment (Figure 7D). Since hepatic ceramides have previously been associated with altered mitochondrial function [61], we subsequently investigated additional lipid classes that may be mechanistically relevant to the relationship between mitochondrial remodeling and hepatic insulin resistance.

Long-chain acylcarnitines, which accumulate when the mitochondrial entry of long-chain fatty acids exceeds their complete oxidation [62], were also reduced by pioglitazone treatment (Figure 7E). Concomitant with the reduced TCA cycle turnover in these mice (Figure 3), this decline in acylcarnitine levels supports an overall reduction in mitochondrial lipid delivery following pioglitazone treatment. Another class of lipids strongly linked to mitochondrial function are the cardiolipins [63]. Total cardiolipin levels were reduced in OB-CON compared to WT mice (Figure 7F). Similarly, levels of hepatic phosphatidic acid, the obligate upstream precursor for cardiolipin, were substantially reduced in OB-CON mice (Supplemental Figure 4B), suggesting that phosphatidic acid depletion could restrict hepatic cardiolipin synthesis in obese mice. Cardiolipin function is closely related to the composition of its four acyl chains, and an optimal tissue cardiolipin profile is believed to consist primarily of mature species containing 3 or 4 18:2 acyl chains [63]. These mature cardiolipins were reduced in livers from OB-CON mice, whereas immature cardiolipin species containing 16:0 and 16:1 acyl chains accumulated (Supplemental Figure 4E). These changes were paralleled by reductions in free linoleic (18:2) acid and in the proportion of linoleic acids in the triglyceride pool (Supplemental Figure 4C and 4D), suggesting that an overall decrease in 18:2 acyl group availability could restrict the remodeling of nascent cardiolipins to their mature counterparts in obese mice livers. Interestingly, cardiolipin species containing longer chain ($\geq$20 carbon) fatty acyl groups, which have previously been linked with pathological cardiolipin remodeling and metabolic dysfunction [63], were markedly increased in OB-CON mice (Figure 7G and Supplemental Figure 4E), as was their contribution to the total cardiolipin pool (Supplemental Figure 4F). This increase in the abundance of long acyl chain cardiolipin species and concomitant reduction in total cardiolipin content was recapitulated in livers from mice fed a high-fat diet (Figure 7H and Supplemental Figure 4G) and was paralleled by increases in long-chain species of lyso-cardiolipin (Figure 7I), a metabolic intermediate of the cardiolipin remodeling process. Notably, although insulin sensitization did not restore levels of total or mature cardiolipin, long chain cardiolipin/lyso-

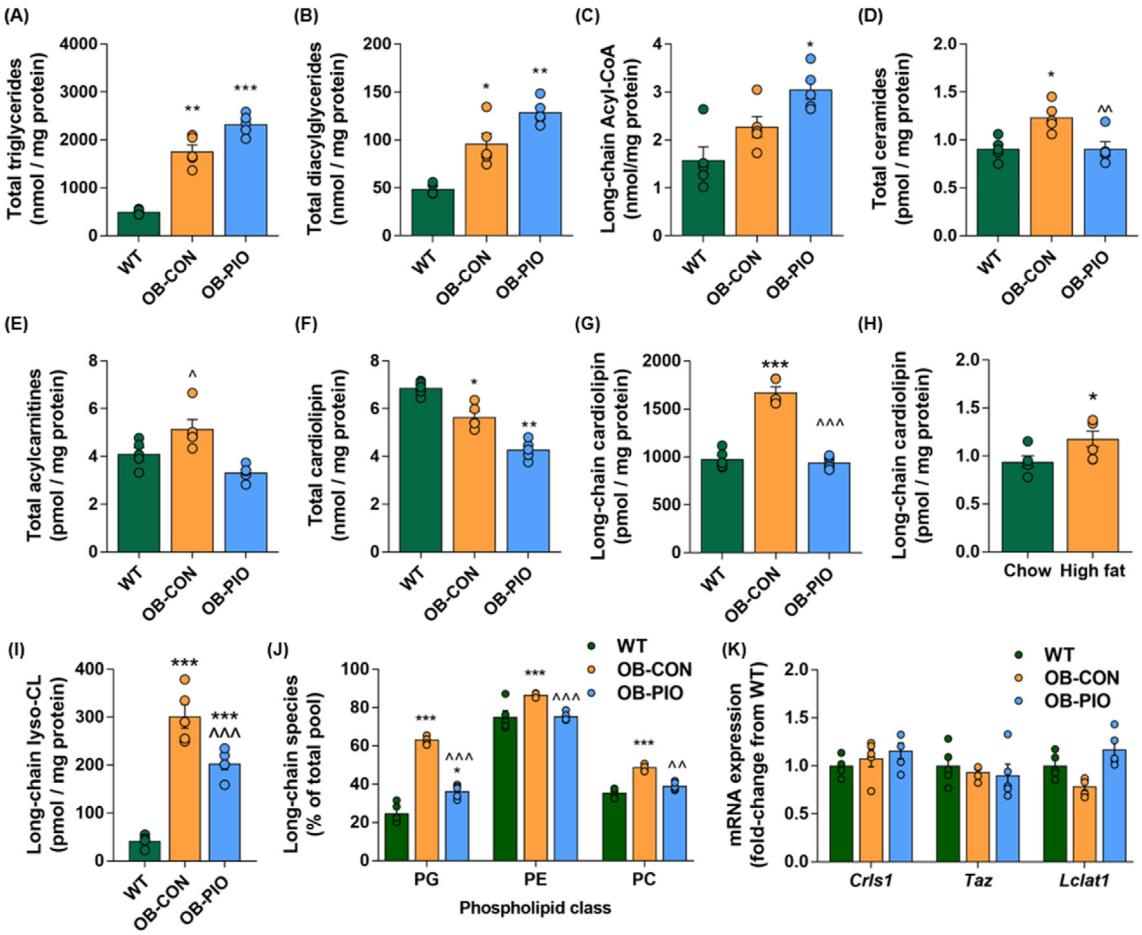

Figure 7: Hepatic insulin sensitization and mitochondrial lipid remodeling. Absolute concentrations of **(A)** triglycerides, **(B)** diacylglycerides, **(C)** long-chain acyl-CoAs, **(D)** ceramides **(E)** long-chain acylcarnitines, **(F)** total cadiolipin, **(G and H)** long-chain cardiolipin, and **(I)** long-chain lyso-cardiolipin, **(J)** relative abundance of long-chain phosphatidylglycerol (PG), phosphatidylethanolamine (PE), and phosphatidylcholine (PC) and **(K)** mRNA expression of cardiolipin synthase 1 (*Crls1*), taffazin (*Taz*), and lysocardiolipin acyltransferase (*Lclat1*) in livers from wild-type (WT), untreated obese mice (OB—CON) and obese mice treated with pioglitazone (25 mg/kg/day) for 4 weeks (OB-PIO) or, for **(H)**, in mice fed a chow or high-fat diet for 9 months. Data are mean ± SE for 5—8 mice per group. *P < 0.05, **P < 0.01, ***P < 0.001 vs WT; ^P<0.05, ^^P<0.01, ^^^P<0.001 vs OB-CON.

cardiolipin species were partially or completely normalized in OB-PIO mice (Figure 7G,I).

To investigate the mechanisms through which pioglitazone prevented the accumulation of pathological cardiolipin species, we analyzed individual species of phosphatidylglycerol (PG), phosphatidylethanolamine (PE), and phosphatidylcholine (PC), since these phospholipids are the primary contributors of fatty acyl chains to the cardiolipin remodeling process [64]. Interestingly, the abundance of phosphotidyl lipid species containing long-chain fatty acyl groups was consistently elevated in OB-CON mice but rescued in OB-PIO mice (Figure 7J and Supplemental Figure 4H). Finally, we measured the expression levels of the key enzymes responsible for cardiolipin generation (cardiolipin synthase 1,[*Crls1*]) and remodeling (tafazzin [*Taz*], and lysocardiolipin acyltransferase 1 [*Lclat1*]). The mRNA levels of these enzymes were unchanged across groups (Figure 7K). These data suggest that the reduction in the availability of substrates for pathological cardiolipin remodeling, rather than the transcriptional regulation of this pathway, drive the hepatic cardiolipin profile in obese mice treated with pioglitazone. In summary, the observed changes in hepatic mitochondrial metabolism in response to insulin sensitizer treatment did not require reductions in bulk liver fat content, but were instead associated with alterations in several distinct lipids closely related to mitochondrial function, including phospholipids involved in pathological cardiolipin remodeling.

4. DISCUSSION

Hallmark pathologies of T2D and NAFLD, such as excessive glucose output and hepatic steatosis, are underpinned by changes in hepatic mitochondrial function. Here, we show that hepatic PDH activity is markedly increased in genetically obese, insulin-resistant mice compared to age-matched lean controls. Activation of PDH in livers from obese mice was attributed, in part, to the coordinated suppression of PDK4 and induction of PDP2. Moreover, increases in hepatic TCA cycle activity, which lower acetyl-CoA concentrations, and excessive glycogenolytic flux, which increase pyruvate concentrations, favor a metabolic milieu that promotes allosteric stimulation of hepatic PDH under insulin resistant conditions. These changes were largely reversed by short-term (4 weeks) treatment of obese mice with the insulin sensitizer pioglitazone. Mechanistically, pioglitazone acutely and directly induced hepatocyte PDK4 in a PPARγ-dependent fashion, providing a crucial link between thiazolidinedione action and mitochondrial metabolism in the liver. Remarkably, improvements in mitochondrial function and insulin sensitivity occurred without reduction in any of the major hepatic lipid classes. Instead, we identify the pathological remodeling of phospholipid cardiolipin as a targetable link between mitochondrial metabolism and hepatic insulin resistance.

It has been suggested that the accelerated TCA cycle flux in insulin-resistant livers reflects the increased energy demands and/or reduced mitochondrial efficiency associated with liver damage [38], although the exact mechanism linking these events has not been delineated. Our data confirm previous reports that elevated rates of TCA cycle turnover in NAFLD and NASH are supported by increases in mitochondrial mass [39] and are associated with lower concentrations of hepatic acetyl-CoA [38]. Notably, this relative depletion of acetyl groups in obese livers is in contrast to the allosteric role of acetyl-CoA as an activator of pyruvate carboxylase flux [65], and suggests that the induction of GNG_{PEP} under insulin-resistant conditions is uncoupled from changes in hepatic acetyl-CoA concentration. However, consistent with the allosteric regulation of PDH by acetyl-CoA [44], we show that the resultant reduction in the hepatic acetyl-CoA/CoASH ratio is associated with increased PDH activation, supporting the increased oxidative demand in these livers. It should be acknowledged that under normal conditions, the contribution of PDH to the hepatic acetyl-CoA pool is relatively minor compared to β-oxidation, such that PDH flux accounts for less than 5% of TCA cycle turnover [66]. Therefore, while absolute rates of PDH flux may be increased in insulin resistant livers, it is unlikely that this can explain the increased rate of TCA cycle turnover observed in NAFLD and NASH patients. Nevertheless, the accelerated mitochondrial acetyl-group delivery from hyperactive PDH represents additional metabolic stress on a system that is already overloaded, and its suppression in OB-PIO mice is further evidence of the normalized regulation of mitochondrial function with pioglitazone. Our finding of increased hepatic PDH activation in obese mice contrasts with a prior report of lower PDH activity in high-fat diet-fed mice [67]. Our conclusions are primarily derived from biochemical assay of PDH activation. However, we also determined the relative ratio between pyruvate carboxylase (PC) and pyruvate dehydrogenase (PDH) fluxes (6 in both OB-CON and OB-PIO fasted mice) which, when combined with our estimations of absolute PC flux (0.7 and 0.37 μmol/min glucose in OB-CON and OB-PIO, respectively), offer a second independent measurement of hepatic PDH flux. Since two molecules of pyruvate are required to form one glucose molecule, absolute PDH flux calculated by this method is approximately 233 and 123 μmol/min for OB-CON and OB-PIO mice, respectively, equivalent to 78 and 34 nmol/g liver/min. These calculations are remarkably similar to the values calculated from our biochemical assay (64 and 33 nmol/g/min) and thus provide independent validation of our measurement of PDH activation. Moreover, the elevated PDH activation in livers from obese mice is further supported by the finding that the main catalytic component of the enzyme complex (PDHE1α) was robustly increased in obese compared to wild-type mice, while its main covalent modulators (PDK4 and PDP2) were altered in a complimentary manner. The reasons for the discrepancy between our results and those of Go et al. [67] are unclear but may reflect differences in the model systems, the severity of hepatic insulin resistance, and/or in the methods used to monitor PDH activity. PDH activity was recently found to be elevated in orthotopic rat hepatomas compared to neighboring liver tissue [68]. As such, our data argue that the induction of PDH in insulin-resistant livers could represent an important, targetable event in the progression from NAFLD and NASH to hepatocellular carcinoma. Paradoxically, pioglitazone downregulates TCA cycle turnover without modulating the PC/PDH ratio. This observation is consistent with the finding that acetyl-CoA moieties are unchanged by pioglitazone treatment

In addition to changes in acetyl-CoA concentrations, the increased PDH activation in obese livers was driven by an increase in the PDH E1α subunit, as well as reduced PDK4 and increased PDP2 protein levels, favoring covalent activation of this subunit. Pioglitazone restored protein levels of PDK4 and PDP2 independently of total E1α protein expression. PDK4 is induced by physiological states of low insulin, including starvation and type I diabetes [69,70], whereas PDP2 is suppressed under such conditions [71]. Therefore, the reciprocal changes in PDP2 observed in OB-CON and OB-PIO mice may be explained by the pioglitazone-mediated improvement in peripheral insulin sensitivity, resulting in lower circulating insulin concentrations. However, PDK4 was also induced by pioglitazone in isolated hepatocytes, suggesting a more direct mode of action. Interestingly, RNA-seq analysis of pioglitazone-treated hepatocytes revealed PDK4 to be the most highly upregulated gene (unpublished data). PDK4 has been extensively studied as a central node in mitochondrial substrate selection and metabolic remodeling [52,72], and the direct induction of

PDK4 by pioglitazone is consistent with previous observations that pioglitazone acutely inhibits pyruvate oxidation [19,73]. We also now show that PPARγ, the primary transcriptional target of the thiazolidinediones [53], is required for this cell-autonomous increase in PDK4 levels. These data challenge the recent concept that the beneficial effects of thiazolidinediones on mitochondrial metabolism can be isolated from their activity as PPARγ ligands, thus calling into question the utility of so-called called PPARγ-sparing thiazolidinediones for the treatment of metabolic disease [74]. Ongoing studies in our laboratory are now exploring the requirement for PPARγ in other direct hepatic effects of pioglitazone.

Our findings suggest that the accelerated rates of oxidative metabolism seen in insulin-resistant livers are supported by changes in mitochondrial number, structure, and function. Intuitively, mitochondrial substrate delivery or partitioning must also be adapted to meet the increased demands of greater TCA cycle turnover. It has been argued that the primary source of this increased substrate delivery is from adipose tissue lipolysis [65] and indeed, the accumulation of long-chain acylcarnitine species observed in the livers of obese mice here indicates excessive mitochondrial lipid delivery. However, our data also suggests that the effects of pioglitazone on mitochondrial function may be distinct from actions on adipose tissue. This is supported by the lack of change in circulating free fatty acids and glycerol, suggesting unaltered lipolysis, as well as the increases in hepatic triglyceride and diacylglyceride contents in OB-PIO mice compared to OB-CON. Instead, we show that disturbed hepatic glycogen metabolism plays an important role in the oversupply of mitochondrial substrates. Insulin-resistant livers were characterized by excessive glycogen storage, persistent glycogenolysis and impaired glycogen synthesis in response to insulin infusion. Pioglitazone restored insulin-stimulated glycogen synthesis and suppressed glycogenolytic flux, which assisted the lowering of hepatic glucose production but also likely restricted glycolytic pyruvate generation. The combination of increased glycogen turnover combined with lower EGP suggests that glycogen cycling may be activated by pioglitazone administration [75]. However, given that complete glucose oxidation produces 36 ATP molecules, whereas glycogen cycling consumes a single ATP for each recycled glucose-1-phosphate, this pathway would have to be very active to significantly alter hepatic energetics [75]. This hypothesis could be directly addressed in the future using the appropriate tracer study. Our observation that the hepatic pyruvate concentration was elevated in obese mice is consistent with the finding that circulating pyruvate concentrations are increased in NAFLD patients [38]. Reducing glycogen-derived pyruvate availability may thus represent a central node linking insulin sensitization with the improvement of mitochondrial function by relieving stimulation of both PDH and PC-mediated TCA cycle substrate delivery.

A previous study found that chronic (6 months) pioglitazone treatment suppressed hepatic TCA cycle flux in a rodent model of NASH, attributing the effects to reduced liver accumulation of triglycerides and diacylglycerides [22]. However, no detailed mechanism was identified for the alteration of mitochondrial function by pioglitazone. Here, we confirm the ability of pioglitazone to slow TCA cycle activity by ^{13}C NMR and corroborate this with decreases in citrate synthase activity, despite no apparent change in mitochondrial mass. This dissociation between hepatic mitochondrial mass and citrate synthase activity has been observed previously in rats with hepatic steatosis and may be indicative of intrinsic changes in mitochondrial structure and/or function [76] with pioglitazone treatment. We also demonstrate that this occurs rapidly (within 4 weeks of treatment) and either precedes or is dissociated from any effects on liver fat content, as major classes of hepatic lipids (triglycerides, diacylglycerides, and free fatty acids) were unchanged by pioglitazone treatment. Instead, we present evidence that the rescue of mitochondrial function by pioglitazone involves remodeling of the mitochondrial lipid cardiolipin. Cardiolipins are a class of inner mitochondrial membrane phospholipids which function to maintain cellular bioenergetics by regulating the organization of mitochondrial proteins [63]. Human data suggest that hepatic levels of total cardiolipin are unchanged [77] or modestly increased [62] in NAFLD and NASH patients. However, the fatty acyl-chain composition of cardiolipin appears to be more important than total content in determining its impact upon hepatic mitochondrial function [78]. As such, a major strength of this work is the use of high-resolution shotgun lipidomics to identify individual cardiolipin species. Our approach revealed a marked reduction in the most abundant cardiolipin species in livers from obese mice, but an increase in many of the less abundant species, particularly those of longer acyl chain length. This pattern of hepatic cardiolipin remodeling recapitulates findings from insulin-resistant cardiac tissue [79] and is reported to promote oxidative stress and mitochondrial dysfunction by rendering cardiolipin more susceptible to peroxidation [80]. Therefore, it seems likely that changes in the content and acyl-chain composition of hepatic cardiolipin likely contribute to the excessive TCA cycle activity and oxidative burden observed in insulin resistant livers. As such, reducing longer acyl-chain cardiolipin species may represent an important mechanism through which insulin sensitization with pioglitazone can protect mitochondria from lipid peroxidation and thus preserve hepatic mitochondrial function.

Two additional classes of lipids that have been closely linked with mitochondrial function in insulin resistant tissues are long-chain acylcarnitines and ceramides. Acylcarnitines are synthesized by carnitine palmitoyltransferase I (CPTI) to facilitate transport of fatty acids into the mitochondria for subsequent β-oxidation [81]. In agreement with evidence from human NASH patients [62,82], total acylcarnitine content was elevated in OB-CON livers, reflecting an imbalance between CPTI-mediated acylcarnitine production and their disposal via β-oxidation. Rates of complete β-oxidation (acetyl-CoA production) were recently shown to be normal in patients with varying severities of NAFLD [38] and therefore it seems likely that the accumulation of hepatic long-chain acylcarnitines reflects increased mitochondrial fatty acid delivery, rather than impaired oxidation. The pioglitazone-induced reduction in acylcarnitines was mirrored by a reduction in hepatic ceramide concentrations, a finding that is consistent with a recent study which reported a lowering of plasma ceramide concentrations in pioglitazone-treated human subjects with metabolic syndrome [83]. Since the patterns of ceramide and cardiolipin remodeling observed here have been directly linked with mitochondrial dysfunction and impaired hepatic β-oxidation [61,79], it is tempting to speculate that the resolution of hepatic acylcarnitine concentrations reflects ceramide and/or cardiolipin-mediated improvements in mitochondrial function. It is also particularly noteworthy that these beneficial alterations in less-abundant hepatic lipid species occurred despite increases in liver triglycerides and diacylglycerides, highlighting the ability of pioglitazone to protect mitochondria from lipid overload even in the setting of increased hepatic lipid storage.

5. CONCLUSIONS

We identify pyruvate dehydrogenase activation and cardiolipin remodeling as novel changes in hepatic mitochondria in insulin-

resistant obese mice. Treatment with pioglitazone reversed these maladaptive processes and improved whole-body glucose metabolism, without reducing hepatic triglyceride levels, suggesting that the link between hepatic lipid storage, mitochondrial function and insulin sensitivity is more nuanced than previously assumed. Hepatic insulin sensitization drives multiple pathways to relieve the oxidative burden of excessive TCA cycle flux and improve mitochondrial function, highlighting the need to target insulin resistance as a primary treatment for liver disease.

AUTHOR CONTRIBUTIONS

Conceptualization, C.E.S., M.R., MEM., and L.N.; Methodology, C.E.S., M.R., MEM., J.P.P., E.S.J., C.R.M., X.H., and L.N.; Formal analysis, C.E.S., M.R., and J.P.P.; Investigation, C.E.S., M.R., M.F., and T.B.; Writing — Original Draft, C.E.S., and L.N.; Writing — Review and Editing, C.E.S., M.R., MEM., J.P.P., M.M., and L.N.; Supervision, MEM. and L.N.; Funding Acquisition, MEM and L.N.

ACKNOWLEDGEMENTS

Project supported by funding from the University of Florida's Southeast Center for Integrated Metabolomics through grant number U24DK097209 from the National Institute of Health's Common Fund metabolomics program. A portion of this work was performed at the National High Magnetic Field Laboratory, which is supported by National Science Foundation Cooperative Agreement number DMR1644779, & the State of Florida, NIH P41-122698, and NIH R01-105346. Additional experiments were performed at Advanced Imaging Center at the University of Texas Southwestern Medical Center, which was supported by an NIH grant P41EB015908. C.E.S. is supported by an UT Health San Antonio OPA Postdoctoral Research Fellowship. A portion of this work was supported by American Diabetes Association Grant 1-15-MI-07 (X.H and J.P.P).

CONFLICT OF INTEREST

The authors declare no competing interests.

APPENDIX A. SUPPLEMENTARY DATA

Supplementary data to this article can be found online at https://doi.org/10.1016/j.molmet.2020.101154.

REFERENCES

[1] Bril, F., Cusi, K., 2017. Management of nonalcoholic fatty liver disease in patients with type 2 diabetes: a call to action. Diabetes Care 40(3):419—430.

[2] Wang, C., Wang, X., Gong, G., Ben, Q., Qiu, W., Chen, Y., et al., 2012. Increased risk of hepatocellular carcinoma in patients with diabetes mellitus: a systematic review and meta-analysis of cohort studies. International Journal of Cancer 130(7):1639—1648.

[3] Bedi, O., Aggarwal, S., Trehanpati, N., Ramakrishna, G., Krishan, P., 2019. Molecular and pathological events involved in the pathogenesis of diabetes-associated nonalcoholic fatty liver disease. Journal of Clinical and Experimental Hepatology 9(5):607—618.

[4] Gaggini, M., Morelli, M., Buzzigoli, E., DeFronzo, R.A., Bugianesi, E., Gastaldelli, A., 2013. Non-alcoholic fatty liver disease (NAFLD) and its connection with insulin resistance, dyslipidemia, atherosclerosis and coronary heart disease. Nutrients 5(5):1544—1560.

[5] Sunny, N.E., Parks, E.J., Browning, J.D., Burgess, S.C., 2011. Excessive hepatic mitochondrial TCA cycle and gluconeogenesis in humans with nonalcoholic fatty liver disease. Cell Metabolism 14(6):804—810.

[6] Schmid, A.I., Szendroedi, J., Chmelik, M., Krssák, M., Moser, E., Roden, M., 2011. Liver ATP synthesis is lower and relates to insulin sensitivity in patients with type 2 diabetes. Diabetes Care 34(2):448—453.

[7] Satapati, S., Sunny, N.E., Kucejova, B., Fu, X., He, T.T., Mendez-Lucas, A., et al., 2012. Elevated TCA cycle function in the pathology of diet-induced hepatic insulin resistance and fatty liver. The Journal of Lipid Research 53(6):1080—1092.

[8] Satapati, S., Kucejova, B., Duarte, J.A., Fletcher, J.A., Reynolds, L., Sunny, N.E., et al., 2016. Mitochondrial metabolism mediates oxidative stress and inflammation in fatty liver. Journal of Clinical Investigation 126(4):1605.

[9] Koliaki, C., Szendroedi, J., Kaul, K., Jelenik, T., Nowotny, P., Jankowiak, F., et al., 2015. Adaptation of hepatic mitochondrial function in humans with non-alcoholic fatty liver is lost in steatohepatitis. Cell Metabolism 21(5):739—746.

[10] Miyazaki, Y., Mahankali, A., Matsuda, M., Glass, L., Mahankali, S., Ferrannini, E., et al., 2001. Improved glycemic control and enhanced insulin sensitivity in type 2 diabetic subjects treated with pioglitazone. Diabetes Care 24(4):710—719.

[11] Bril, F., Kalavalapalli, S., Clark, V.C., Lomonaco, R., Soldevila-Pico, C., Liu, I.C., et al., 2018. Response to pioglitazone in patients with nonalcoholic steatohepatitis with vs without type 2 diabetes. Clinical Gastroenterology and Hepatology 16(4):558—566 e2.

[12] Cusi, K., Orsak, B., Bril, F., Lomonaco, R., Hecht, J., Ortiz-Lopez, C., et al., 2016. Long-term pioglitazone treatment for patients with nonalcoholic steatohepatitis and prediabetes or type 2 diabetes mellitus: a randomized trial. Annals of Internal Medicine 165(5):305—315.

[13] Miyazaki, Y., Matsuda, M., DeFronzo, R.A., 2002. Dose-response effect of pioglitazone on insulin sensitivity and insulin secretion in type 2 diabetes. Diabetes Care 25(3):517—523.

[14] DeFronzo, R.A., Tripathy, D., Schwenke, D.C., Banerji, M., Bray, G.A., Buchanan, T.A., et al., 2011. Pioglitazone for diabetes prevention in impaired glucose tolerance. New England Journal of Medicine 364(12):1104—1115.

[15] Belfort, R., Harrison, S.A., Brown, K., Darland, C., Finch, J., Hardies, J., et al., 2006. A placebo-controlled trial of pioglitazone in subjects with nonalcoholic steatohepatitis. New England Journal of Medicine 355(22):2297—2307.

[16] Spiegelman, B.M., 1998. PPAR-gamma: adipogenic regulator and thiazolidinedione receptor. Diabetes 47(4):507—514.

[17] Bays, H., Mandarino, L., DeFronzo, R.A., 2004. Role of the adipocyte, free fatty acids, and ectopic fat in pathogenesis of type 2 diabetes mellitus: peroxisomal proliferator-activated receptor agonists provide a rational therapeutic approach. Journal of Clinical Endocrinology & Metabolism 89(2):463—478.

[18] Miyazaki, Y., DeFronzo, R.A., 2008. Rosiglitazone and pioglitazone similarly improve insulin sensitivity and secretion, glucose tolerance and adipocytokines in type 2 diabetic patients. Diabetes, Obesity and Metabolism 10(12):1204—1211.

[19] Shannon, C.E., Daniele, G., Galindo, C., Abdul-Ghani, M.A., DeFronzo, R.A., Norton, L., 2017. Pioglitazone inhibits mitochondrial pyruvate metabolism and glucose production in hepatocytes. FEBS Journal 284(3):451—465.

[20] Raman, P., Judd, R.L., 2000. Role of glucose and insulin in thiazolidinedione-induced alterations in hepatic gluconeogenesis. European Journal of Pharmacology 409(1):19—29.

[21] Nishimura, Y., Inoue, Y., Takeuchi, H., Oka, Y., 1997. Acute effects of pioglitazone on glucose metabolism in perfused rat liver. Acta Diabetologica 34(3):206—210.

[22] Kalavalapalli, S., Bril, F., Koelmel, J.P., Abdo, K., Guingab, J., Andrews, P., et al., 2018. Pioglitazone improves hepatic mitochondrial function in a mouse model of nonalcoholic steatohepatitis. American Journal of Physiology. Endocrinology and Metabolism 315(2):E163—E173.

[23] McCommis, K.S., Chen, Z., Fu, X., McDonald, W.G., Colca, J.R., Kletzien, R.F., et al., 2015. Loss of mitochondrial pyruvate carrier 2 in the liver leads to defects in gluconeogenesis and compensation via pyruvate-alanine cycling. Cell Metabolism 22(4):682—694.

[24] Srere, P.A., 1969. Citrate synthase. Methods in Enzymology 13:3—11.
[25] Han, X., Yang, K., Yang, J., Cheng, H., Gross, R.W., 2006. Shotgun lipidomics of cardiolipin molecular species in lipid extracts of biological samples. The Journal of Lipid Research 47(4):864—879.
[26] Wang, C., Liu, F., Frisch-Daiello, J.L., Martin, S., Patterson, T.A., Gu, Q., et al., 2018. Lipidomics reveals a systemic energy deficient state that precedes neurotoxicity in neonatal monkeys after sevoflurane exposure. Analytica Chimica Acta 1037:87—96.
[27] Wang, M., Wang, C., Han, X., 2017. Selection of internal standards for accurate quantification of complex lipid species in biological extracts by electrospray ionization mass spectrometry-What, how and why? Mass Spectrometry Reviews 36(6):693—714.
[28] Yang, K., Cheng, H., Gross, R.W., Han, X., 2009. Automated lipid identification and quantification by multidimensional mass spectrometry-based shotgun lipidomics. Analytical Chemistry 81(11):4356—4368.
[29] Ramaswamy, V., Hooker, J.W., Withers, R.S., Nast, R.E., Brey, W.W., Edison, A.S., 2013. Development of a ^{13}C-optimized 1.5-mm high temperature superconducting NMR probe. Journal of Magnetic Resonance 235:58—65.
[30] Merritt, M., Bretthorst, G.L., Burgess, S.C., Sherry, A.D., Malloy, C.R., 2003. Sources of plasma glucose by automated Bayesian analysis of 2H NMR spectra. Magnetic Resonance in Medicine 50(4):659—663.
[31] Constantin-Teodosiu, D., Cederblad, G., Hultman, E., 1991. A sensitive radioisotopic assay of pyruvate dehydrogenase complex in human muscle tissue. Analytical Biochemistry 198(2):347—351.
[32] Shannon, C., Merovci, A., Xiong, J., Tripathy, D., Lorenzo, F., McClain, D., et al., 2018. Effect of chronic hyperglycemia on glucose metabolism in subjects with normal glucose tolerance. Diabetes 67(12):2507—2517.
[33] Cederblad, G., Carlin, J.I., Constantin-Teodosiu, D., Harper, P., Hultman, E., 1990. Radioisotopic assays of CoASH and carnitine and their acetylated forms in human skeletal muscle. Analytical Biochemistry 185(2):274—278.
[34] Harris, R.C., Hultman, E., Nordesjö, L.O., 1974. Glycogen, glycolytic intermediates and high-energy phosphates determined in biopsy samples of musculus quadriceps femoris of man at rest. Methods and variance of values. Scandinavian Journal of Clinical & Laboratory Investigation 33(2): 109—120.
[35] Aronoff, S., Rosenblatt, S., Braithwaite, S., Egan, J.W., Mathisen, A.L., Schneider, R.L., 2000. Pioglitazone hydrochloride monotherapy improves glycemic control in the treatment of patients with type 2 diabetes: a 6-month randomized placebo-controlled dose-response study. The Pioglitazone 001 Study Group. Diabetes Care 23(11):1605—1611.
[36] Hausler, N., Browning, J., Merritt, M., Storey, C., Milde, A., Jeffrey, F.M., et al., 2006. Effects of insulin and cytosolic redox state on glucose production pathways in the isolated perfused mouse liver measured by integrated 2H and 13C NMR. Biochemical Journal 394(Pt 2):465—473.
[37] Edgerton, D.S., Kraft, G., Smith, M., Farmer, B., Williams, P.E., Coate, K.C., et al., 2017. Insulin's direct hepatic effect explains the inhibition of glucose production caused by insulin secretion. JCI Insight 2(6):e91863.
[38] Fletcher, J.A., Deja, S., Satapati, S., Fu, X., Burgess, S.C., Browning, J.D., 2019. Impaired ketogenesis and increased acetyl-CoA oxidation promote hyperglycemia in human fatty liver. JCI Insight 5.
[39] Garcia, J., Decker, C.W., Sanchez, S.J., Ouk, J.M., Siu, K.M., Han, D., 2018. Obesity and steatosis promotes mitochondrial remodeling that enhances respiratory capacity in the liver of ob/ob mice. FEBS Letters 592(6):916—927.
[40] Krebs, H.A., 1970. Rate control of the tricarboxylic acid cycle. Advances in Enzyme Regulation 8:335—353.
[41] Burgess, S.C., Jeffrey, F.M., Storey, C., Milde, A., Hausler, N., Merritt, M.E., et al., 2005. Effect of murine strain on metabolic pathways of glucose production after brief or prolonged fasting. American Journal of Physiology-Endocrinology and Metabolism 289(1):E53—E61.
[42] Jin, E.S., Jones, J.G., Merritt, M., Burgess, S.C., Malloy, C.R., Sherry, A.D., 2004. Glucose production, gluconeogenesis, and hepatic tricarboxylic acid cycle fluxes measured by nuclear magnetic resonance analysis of a single glucose derivative. Analytical Biochemistry 327(2):149—155.
[43] Jin, E.S., Moreno, K.X., Wang, J.X., Fidelino, L., Merritt, M.E., Sherry, A.D., et al., 2016. Metabolism of hyperpolarized [1-(13)C]pyruvate through alternate pathways in rat liver. NMR in Biomedicine 29(4):466—474.
[44] Batenburg, J.J., Olson, M.S., 1976. Regulation of pyruvate dehydrogenase by fatty acid in isolated rat liver mitochondria. Journal of Biological Chemistry 251(5):1364—1370.
[45] Carlin, J.I., Harris, R.C., Cederblad, G., Constantin-Teodosiu, D., Snow, D.H., Hultman, E., 1985. Association between muscle acetyl-CoA and acetylcarnitine levels in the exercising horse. Journal of Applied Physiology 69(1):42—45, 1990.
[46] Cate, R.L., Roche, T.E., 1978. A unifying mechanism for stimulation of mammalian pyruvate dehydrogenase(a) kinase by reduced nicotinamide adenine dinucleotide, dihydrolipoamide, acetyl coenzyme A, or pyruvate. Journal of Biological Chemistry 253(2):496—503.
[47] d'Avignon, D.A., Puchalska, P., Ercal, B., Chang, Y., Martin, S.E., Graham, M.J., et al., 2018. Hepatic ketogenic insufficiency reprograms hepatic glycogen metabolism and the lipidome. JCI Insight 3(12).
[48] Turner, S.M., Linfoot, P.A., Neese, R.A., Hellerstein, M.K., 2005. Sources of plasma glucose and liver glycogen in fasted ob/ob mice. Acta Diabetologica 42(4):187—193.
[49] Jeoung, N.H., Wu, P., Joshi, M.A., Jaskiewicz, J., Bock, C.B., Depaoli-Roach, A.A., et al., 2006. Role of pyruvate dehydrogenase kinase isoenzyme 4 (PDHK4) in glucose homoeostasis during starvation. Biochemical Journal 397(3):417—425.
[50] Huang, B., Gudi, R., Wu, P., Harris, R.A., Hamilton, J., Popov, K.M., 1998. Isoenzymes of pyruvate dehydrogenase phosphatase. DNA-derived amino acid sequences, expression, and regulation. Journal of Biological Chemistry 273(28):17680—17688.
[51] Chao, L., Marcus-Samuels, B., Mason, M.M., Moitra, J., Vinson, C., Arioglu, E., et al., 2000. Adipose tissue is required for the antidiabetic, but not for the hypolipidemic, effect of thiazolidinediones. Journal of Clinical Investigation 106(10):1221—1228.
[52] Zhang, S., Hulver, M.W., McMillan, R.P., Cline, M.A., Gilbert, E.R., 2014. The pivotal role of pyruvate dehydrogenase kinases in metabolic flexibility. Nutrition and Metabolism 11(1):10.
[53] Lehmann, J.M., Moore, L.B., Smith-Oliver, T.A., Wilkison, W.O., Willson, T.M., Kliewer, S.A., 1995. An antidiabetic thiazolidinedione is a high affinity ligand for peroxisome proliferator-activated receptor gamma (PPAR gamma). Journal of Biological Chemistry 270(22):12953—12956.
[54] Tontonoz, P., Hu, E., Graves, R.A., Budavari, A.I., Spiegelman, B.M., 1994. mPPAR gamma 2: tissue-specific regulator of an adipocyte enhancer. Genes & Development 8(10):1224—1234.
[55] Vidal-Puig, A., Jimenez-Linan, M., Lowell, B.B., Hamann, A., Hu, E., Spiegelman, B., et al., 1996. Regulation of PPAR gamma gene expression by nutrition and obesity in rodents. Journal of Clinical Investigation 97(11):2553—2561.
[56] Edvardsson, U., Bergström, M., Alexandersson, M., Bamberg, K., Ljung, B., Dahllöf, B., 1999. Rosiglitazone (BRL49653), a PPARgamma-selective agonist, causes peroxisome proliferator-like liver effects in obese mice. The Journal of Lipid Research 40(7):1177—1184.
[57] Pettinelli, P., Videla, L.A., 2011. Up-regulation of PPAR-gamma mRNA expression in the liver of obese patients: an additional reinforcing lipogenic mechanism to SREBP-1c induction. Journal of Clinical Endocrinology & Metabolism 96(5):1424—1430.
[58] Matsusue, K., Haluzik, M., Lambert, G., Yim, S.H., Gavrilova, O., Ward, J.M., et al., 2003. Liver-specific disruption of PPARgamma in leptin-deficient mice improves fatty liver but aggravates diabetic phenotypes. Journal of Clinical Investigation 111(5):737—747.
[59] Bajaj, M., Suraamornkul, S., Pratipanawatr, T., Hardies, L.J., Pratipanawatr, W., Glass, L., et al., 2003. Pioglitazone reduces hepatic fat

content and augments splanchnic glucose uptake in patients with type 2 diabetes. Diabetes 52(6):1364–1370.

[60] Yki-Jarvinen, H., 2004. Thiazolidinediones. New England Journal of Medicine 351(11):1106–1118.

[61] Raichur, S., Wang, S.T., Chan, P.W., Li, Y., Ching, J., Chaurasia, B., et al., 2014. CerS2 haploinsufficiency inhibits β-oxidation and confers susceptibility to diet-induced steatohepatitis and insulin resistance. Cell Metabolism 20(4):687–695.

[62] Peng, K.Y., Watt, M.J., Rensen, S., Greve, J.W., Huynh, K., Jayawardana, K.S., et al., 2018. Mitochondrial dysfunction-related lipid changes occur in nonalcoholic fatty liver disease progression. The Journal of Lipid Research 59(10):1977–1986.

[63] He, Q., Han, X., 2014. Cardiolipin remodeling in diabetic heart. Chemistry and Physics of Lipids 179:75–81.

[64] Kiebish, M.A., Bell, R., Yang, K., Phan, T., Zhao, Z., Ames, W., et al., 2010. Dynamic simulation of cardiolipin remodeling: greasing the wheels for an interpretative approach to lipidomics. The Journal of Lipid Research 51(8): 2153–2170.

[65] Perry, R.J., Camporez, J.G., Kursawe, R., Titchenell, P.M., Zhang, D., Perry, C.J., et al., 2015. Hepatic acetyl CoA links adipose tissue inflammation to hepatic insulin resistance and type 2 diabetes. Cell 160(4):745–758.

[66] Cappel, D.A., Deja, S., Duarte, J.A.G., Kucejova, B., Inigo, M., Fletcher, J.A., et al., 2019. Pyruvate-carboxylase-mediated anaplerosis promotes antioxidant capacity by sustaining TCA cycle and redox metabolism in liver. Cell Metabolism 29(6):1291–12305 e8.

[67] Go, Y., Jeong, J.Y., Jeoung, N.H., Jeon, J.H., Park, B.Y., Kang, H.J., et al., 2016. Inhibition of pyruvate dehydrogenase kinase 2 protects against hepatic steatosis through modulation of tricarboxylic acid cycle anaplerosis and ketogenesis. Diabetes 65(10):2876–2887.

[68] Lee, M.H., DeBerardinis, R.J., Wen, X., Corbin, I.R., Sherry, A.D., Malloy, C.R., et al., 2019. Active pyruvate dehydrogenase and impaired gluconeogenesis in orthotopic hepatomas of rats. Metabolism 101:153993.

[69] Huang, B., Wu, P., Bowker-Kinley, M.M., Harris, R.A., 2002. Regulation of pyruvate dehydrogenase kinase expression by peroxisome proliferator-activated receptor-alpha ligands, glucocorticoids, and insulin. Diabetes 51(2):276–283.

[70] Wu, P., Blair, P.V., Sato, J., Jaskiewicz, J., Popov, K.M., Harris, R.A., 2000. Starvation increases the amount of pyruvate dehydrogenase kinase in several mammalian tissues. Archives of Biochemistry and Biophysics 381(1):1–7.

[71] Huang, B., Wu, P., Popov, K.M., Harris, R.A., 2003. Starvation and diabetes reduce the amount of pyruvate dehydrogenase phosphatase in rat heart and kidney. Diabetes 52(6):1371–1376.

[72] Park, S., Jeon, J.H., Min, B.K., Ha, C.M., Thoudam, T., Park, B.Y., et al., 2018. Role of the pyruvate dehydrogenase complex in metabolic remodeling: differential pyruvate dehydrogenase complex functions in metabolism. Diabetes & Metabolism J 42(4):270–281.

[73] Divakaruni, A.S., Wiley, S.E., Rogers, G.W., Andreyev, A.Y., Petrosyan, S., Loviscach, M., et al., 2013. Thiazolidinediones are acute, specific inhibitors of the mitochondrial pyruvate carrier. Proceedings of the National Academy of Sciences of the U S A 110(14):5422–5427.

[74] Chen, Z., Vigueira, P.A., Chambers, K.T., Hall, A.M., Mitra, M.S., Qi, N., et al., 2012. Insulin resistance and metabolic derangements in obese mice are ameliorated by a novel peroxisome proliferator-activated receptor γ-sparing thiazolidinedione. Journal of Biological Chemistry 287(28):23537–23548.

[75] Landau, B.R., 2001. Methods for measuring glycogen cycling. American Journal of Physiology. Endocrinology and Metabolism 281(3):E413–E419.

[76] Raffaella, C., Francesca, B., Italia, F., Marina, P., Giovanna, L., Susanna, I., 2008. Alterations in hepatic mitochondrial compartment in a model of obesity and insulin resistance. Obesity 16(5):958–964.

[77] Puri, P., Baillie, R.A., Wiest, M.M., Mirshahi, F., Choudhury, J., Cheung, O., et al., 2007. A lipidomic analysis of nonalcoholic fatty liver disease. Hepatology 46(4):1081–1090.

[78] Cole, L.K., Mejia, E.M., Vandel, M., Sparagna, G.C., Claypool, S.M., Dyck-Chan, L., et al., 2016. Impaired cardiolipin biosynthesis prevents hepatic steatosis and diet-induced obesity. Diabetes 65(11):3289–3300.

[79] Han, X., Yang, J., Yang, K., Zhao, Z., Abendschein, D.R., Gross, R.W., 2007. Alterations in myocardial cardiolipin content and composition occur at the very earliest stages of diabetes: a shotgun lipidomics study. Biochemistry 46(21):6417–6428.

[80] Li, J., Romestaing, C., Han, X., Li, Y., Hao, X., Wu, Y., et al., 2010. Cardiolipin remodeling by ALCAT1 links oxidative stress and mitochondrial dysfunction to obesity. Cell Metabolism 12(2):154–165.

[81] Fritz, I.B., Yue, K.T., 1963. Long-chain carnitine acyltransferase and the role OF acylcarnitine derivatives IN the catalytic increase OF fatty acid oxidation induced BY carnitine. The Journal of Lipid Research 4:279–288.

[82] Pérez-Carreras, M., Del Hoyo, P., Martín, M.A., Rubio, J.C., Martín, A., Castellano, G., et al., 2003. Defective hepatic mitochondrial respiratory chain in patients with nonalcoholic steatohepatitis. Hepatology 38(4):999–1007.

[83] Warshauer, J.T., Lopez, X., Gordillo, R., Hicks, J., Holland, W.L., Anuwe, E., et al., 2015. Effect of pioglitazone on plasma ceramides in adults with metabolic syndrome. Diabetes/Metabolism Research and Reviews 31(7):734–744.

